RESPIRATORY EFFECTS OF GENERAL ANESTHESIA AND PULMONARY EMBOLISM IN RODENT MODELS

Bence Ballók MD

PhD Thesis

Szeged

2024

University of Szeged, Hungary

Albert Szent-Györgyi Medical School

Doctoral School of Interdisciplinary Medicine

RESPIRATORY EFFECTS OF GENERAL ANESTHESIA AND PULMONARY EMBOLISM IN RODENT MODELS

PhD Thesis

Bence Ballók MD

Department of Medical Physics and Informatics

Supervisors:

Prof. Ferenc Peták PhD DSc

Gergely Fodor MD PhD

Szeged,

2024

1. List of scientific publications included in the present thesis:

I.   **Comparison of the respiratory effects of commonly utilized general anesthesia regimes in male Sprague-Dawley rats**

Bence Ballók, Álmos Schranc, Ibolya Tóth, Petra Somogyi, József Tolnai, Ferenc Peták, Gergely H Fodor

Frontiers in Physiology, 2023; 14: 1249127   IF: 3.2   SJR ranking: Q2

II.   **Changes in lung mechanics and ventilation-perfusion match: comparison of pulmonary air- and thromboembolism in rats**

József Tolnai, Bence Ballók, Roberta Südy, Álmos Schranc, Gabriella Varga, Barna Babik, Gergely H Fodor, Ferenc Peták

BMC Pulmonary Medicine, 2024; 24(1):27   IF: 2.6   SJR ranking: Q2

Scientific publication related to the subject of the present thesis:

III.   **Lung and chest wall mechanical properties in metformin-treated and untreated models of type 2 diabetes**

Álmos Schranc, Gergely H. Fodor, Roberta Südy, Bence Ballók, Richard Kulcsár, József Tolnai, Barna Babik, Ferenc Peták

Journal of Applied Physiology, 2022; 132(5):1115-1124   IF: 3.3 SJR ranking: Q1

2. Table of contents

3. Figures and tables

4. List of abbreviations

AE: air embolism

ANOVA: analyses of variance

ARRIVE: Animal Research: Reporting of In Vivo Experiments

AVDSf: alveolar dead space fraction

$ED100_{Raw}$: methacholine dose needed for 100% elevation of airway resistance

EELV: end-expiratory lung volume

$ETCO_2$: end-tidal carbon dioxide concentration

FOT: forced oscillation technique

G: tissue damping

H: tissue elastance

HR: heart rate

Iaw: airway inertance

ip: intraperitoneal

iv: intravenous

KX: ketamine-xylazine

LPAO: left pulmonary artery occlusion

MAC: minimum alveolar concentration

MAP: mean arterial pressure

MCh: methacholine

$PaCO_2$: arterial partial pressures of carbon dioxide

PaO_2: arterial partial pressures of oxygen

PB: sodium pentobarbital

PCO_2: partial pressure of carbon dioxide

PEEP: positive end-expiratory pressure

PF: propofol and fentanyl

Ptr: pressure measured inside the trachea

Raw: airway resistance

S: sevoflurane

Sn2V: normalized phase 2 slope of the volumetric capnogram

Sn3V: normalized phase 3 slope of the volumetric capnogram

U: urethane

VDB: Bohr's physiological dead space

VDE: Enghoff's modified physiological dead space

VDF: Fowler's anatomic dead space

VT: tidal volume

Zrs: input impedance of the respiratory system

η: tissue hysteresivity

5. Introduction

5.1. Anesthesia

Anesthesia is essential for a wide variety of medical procedures to relieve pain and provide optimal conditions for surgical interventions and intensive care. The type and extent of anesthesia required vary depending on the specific intervention. In medical practice, there are several types of anesthesia: local anesthesia is used for minor procedures, it anesthetizes a small part of the body. Regional anesthesia targets larger body areas, such as limbs, without affecting the patient's consciousness. General anesthesia involves administering various anesthetics to induce a loss of consciousness, often requiring mechanical ventilation.

General anesthesia plays a crucial role in medical sciences and is, therefore, the subject of extensive research. A significant focus of these studies is the investigation of the pulmonary aspects of anesthetic interventions. Experimental research frequently necessitates the use of general anesthesia [3]. However, it is well-established that general anesthesia has a significant impact on the respiratory system [4], primarily due to respiratory depression or altered breathing patterns resulting from disrupted control of breathing and loss of respiratory muscle tone [5]. These factors can lead to the rapid formation of atelectasis and airway closure, resulting in reduced functional residual capacity, hypoxia, hypercapnia and increased intrapulmonary shunting [5; 6; 7]. These blood gas abnormalities may also affect bronchial and pulmonary vascular functions, ultimately altering respiratory mechanics [5; 6]. Mechanical ventilation can mitigate these effects, preventing most of these complications [7; 8].

Agents used for general anesthesia can have various direct and indirect effects on the respiratory system. Several studies have demonstrated the bronchodilator effects of volatile anesthetics in both animal and human models [9; 10; 11; 12]. However, other studies have reported serious respiratory adverse effects associated with certain anesthetic drugs, such as xylazine-induced pulmonary edema and surfactant dysfunction [13; 14]. Xylazine is commonly used for sedation alone or in combination with ketamine for general anesthesia. The effects of other anesthetic agents on respiratory function and mechanics have not been fully characterized yet.

5.2. Patient monitoring

Monitoring vital signs during medical interventions and intensive care is of paramount importance. It enables the early detection of severe deteriorations in a patient's condition, thereby contributing to the prevention of adverse effects and enhancing patient safety and outcomes. Depending on the medical procedure, patient monitoring can range from simple measurements of vital signs to more sophisticated approaches, with several guidelines available to standardize the level of monitoring required for different procedures [15]. Systems, such as anesthesia machine platforms, display numerous vital parameters, facilitating decision-making for medical professionals. Monitoring systems can display cardiovascular and respiratory parameters such as blood pressure, oxygen saturation, ECG, heart rate, the composition of the inspired gas mixture, airflow, airway pressure, capnograms, and EEG activity.

5.3. Respiratory monitoring: capnography

Capnography is an essential tool in patient monitoring, particularly in respiratory care. This technique offers a non-invasive, continuous analysis of exhaled carbon dioxide, providing both numerical data and graphical representations [16]. It operates primarily using two methods: the qualitative approach with colorimetry [16; 17] or, more commonly, the quantitative approach through infrared spectroscopy [16; 18].
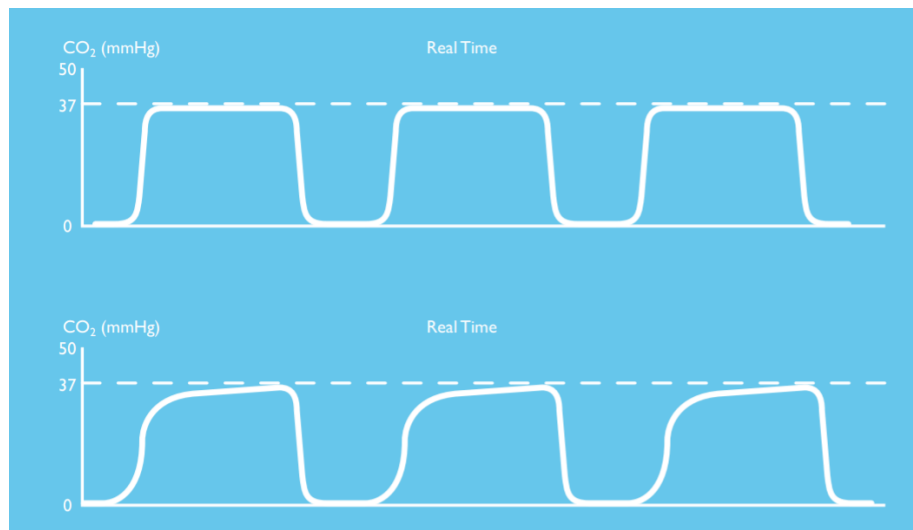
Figure 1 Mainstream (upper) and sidestream (lower) capnogram curve

(source: https://bionetus.com/vet/capnography/etco2-sensor-ss/)

Capnography can be categorized based on where the carbon dioxide measurement occurs: it can be mainstream or sidestream. In mainstream capnography, the measuring device is placed

between the ventilator tubing and the Y-piece of the ventilation system [19], ensuring rapid and precise data collection but with the drawback of increasing the dead space [20]. On the other hand, sidestream capnography samples the gas continuously from the measurement site [19], allowing the measurement of multiple gases besides CO_2.

There are also distinctions in how the CO_2 concentration is displayed: time-based and
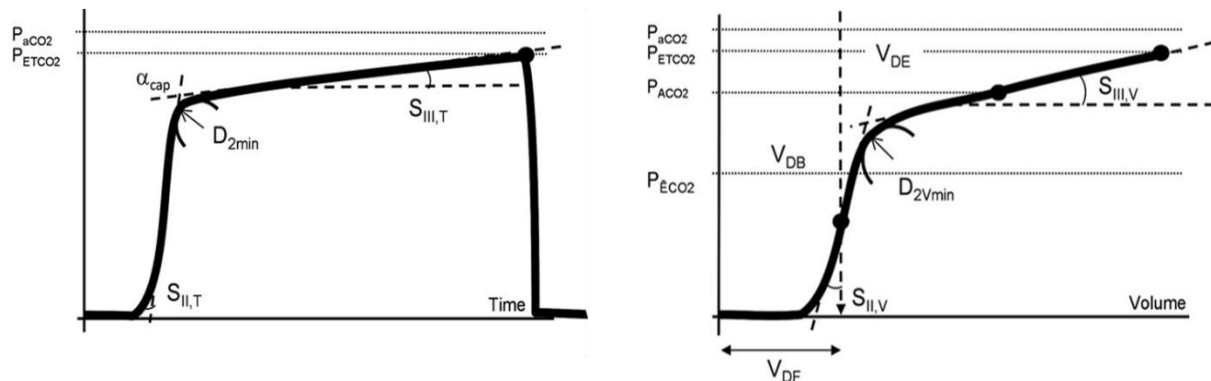
Figure 2 Schematic diagram of time and volumetric capnogram curves (source: [1])

P_{aCO_2}: mean alveolar carbon dioxide concentration at the midpoint of phase III of carbon dioxide expiration; P_{ETCO_2}: ; α_{cap}=angle formed by the phase II and phase III limbs of the expiratory time capnogram; D_{2min} and D_{2Vmin} = curvature at the phase II to phase III transitions, calculated as the minimum of the second-order time and volumetric derivative, respectively; SII,T: phase 2 slope time capnogram; SIII,T: phase 3 slope of time capnogram; SII,V: phase 2 slope of volumetric capnogram; SIII,V: phase 3 slope of volumetric capnogram; V_{DF}: anatomic dead space according to Fowler

volumetric capnography. Time capnography graphs the exhaled CO_2 against time, which helps in identifying intubation issues or blockages in the tube. Volumetric capnography, meanwhile, measures the CO_2 output per breath, requiring flow measurement and offering the advantage of identifying ventilation dead spaces.

The capnogram curve is typically divided into three phases [21]. Phase 1 marks the beginning of exhalation, where the exhaled gas leaves the conducting airways. Phase 2 shows the transition zone, where gas from both the alveoli and conducting airways mixes [16; 22]. Phase 3 reflects the CO_2 content of the alveolar gas, displayed as a steadily rising plateau, with the highest point indicating the end-tidal CO_2 concentration. At the end of phase 3, inhalation begins and the capnogram curve returns to the baseline.
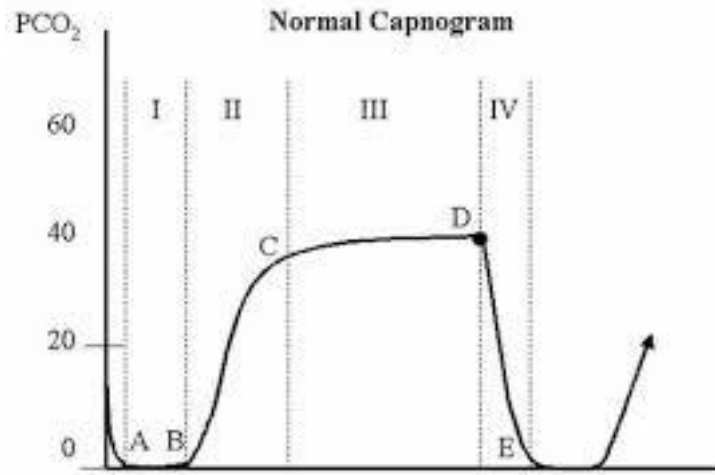
Figure 3 Capnogram curve (source: [2])

A: start of exhalation; A-B: air from the conductive airways; B-C: mixed air from conductive airways and alveoli; C-D: exhaled air from alveoli; D: end of expiration, end-expiratory CO_2; D-E: inhalation; I: phase 1; II: phase 2; III: phase 3; IV: inhalation

Deviations in the capnogram curve could also suggest tube leakage, soda exhaustion, obstructions (Figure 4), or improper intubation, among other potential complications, also we can infer to the depth of anesthesia and the cessation of the muscle relaxant.
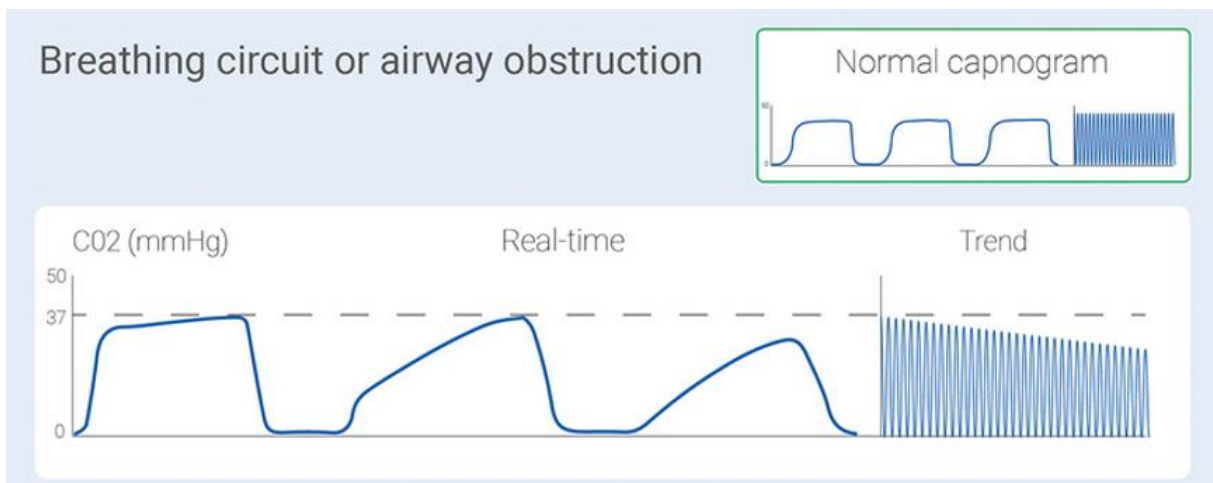
Figure 4 Schematic diagram of capnogram curve during airway obstruction

(source: https://www.slideshare.net/slideshow/capnography-vs-plethysmography/73724225)

5.4. Pulmonary embolism

Embolism is a life-threatening cardiovascular event, that occurs when an embolus gets lodged in the circulatory system and causes a circulation disorder. It ranks third in causes of cardiovascular death worldwide, following stroke and myocardial ischemia [23]. First described by Virchow in the 1800s, it was often associated with fatal outcomes [24].

Diagnosing pulmonary embolism is challenging for clinicians due to its highly variable clinical symptoms [25], with the most common being pleuritic chest pain, dyspnea at rest, tachypnea, tachycardia, and hypoxia [23; 24]. Laboratory tests (especially D-dimer), ultrasound, chest CT, and analysis of end-tidal CO_2 levels and the capnogram curve can assist in the diagnosis. Additionally, various clinical guidelines, such as the Wells score system, which assigns up to 12.5 points based on multiple clinical features (with a score above 4 points making pulmonary embolism likely and recommending imaging), are useful diagnostic tools [24].

Embolisms can be categorized based on their formation. Fat embolism, typically following fractures of long bones, involves fat droplets causing the blockage. Fluid embolism, a rare type, mostly occurs during childbirth when amniotic fluid enters the bloodstream. Two more common types are pulmonary thromboembolism, where a blood clot (mostly from deep veins in the lower limbs) lodges in the arteries of the pulmonary system, and air/gas embolism, where an air bubble blocks the vascular system (often iatrogenic).

Although both pulmonary gas embolism and thromboembolism compromise pulmonary blood flow, they differ substantially, particularly in the regional distribution of pulmonary perfusion defects. Gas bubbles in venous blood undergo turbulent mixing and disruption in the right ventricle, leading primarily to gravity-dependent diffuse pulmonary hypoperfusion [26; 27; 28]. In contrast, the spatial distribution of thromboembolism is more focal, primarily affecting distinct lung areas [29; 30; 31]. These fundamental differences in the spatial distribution of lung perfusion defects may influence adverse changes in respiratory mechanics, gas exchange, and ventilation-perfusion matching. Consequently, significant differences in outcomes can be expected between these two forms of embolism.

Treatment for pulmonary embolism may vary according to the severity of the condition. The primary therapies include anticoagulation (with low-molecular-weight heparin), thrombolysis, or thrombectomy, but close observation of the patient is recommended in all cases [24].

5.5. Forced Oscillation Technique

Forced oscillation technique (FOT) is a method of respiratory function testing that also allows for the study of respiratory mechanics. Its primary advantage is that it requires little or no cooperation from the patient, or in our case, the experimental animal.

FOT measurements typically use a loudspeaker to generate external pressure signals that are superimposed on the normal breathing pattern in spontaneously breathing subjects. These pressure signals are delivered to the respiratory system while the oscillatory airflow and airway opening pressures are measured. Airflow measurement can be performed with a screen pneumotachograph based on the Hagen-Poiseuille equation, a Pitot tube based on Bernoulli's principle, or even with ultrasonic measurement following the Doppler principle. By integrating the measured airflow signal, the area under the resulting curve corresponds to the gas volume.
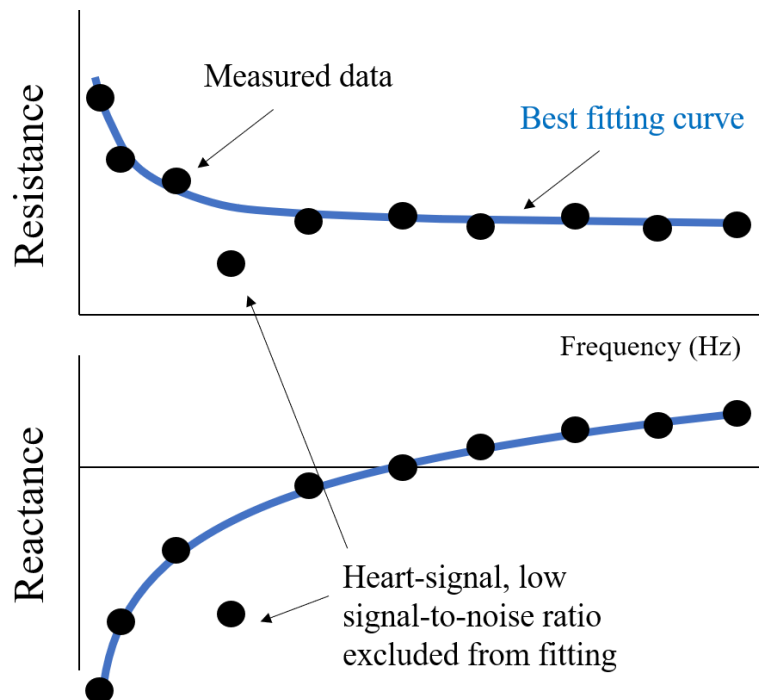
Figure 5 Representative spectrum of FOT measurements

From the spectral analysis of the pressure and flow signals, the real part of the impedance reflects the resistive properties (airway and tissue components), while the imaginary part provides information on the respiratory system's elastic and inertive forces. By fitting a mathematical model to the complex impedance spectra, physiologically relevant mechanical parameters of the respiratory system can be identified.

The low-frequency real part primarily determines the frequency-dependent tissue resistance (G), which reflects the internal energy loss of the respiratory tissues. The low-frequency imaginary part mainly represents the respiratory tissue elasticity (H). The ratio of these two values infers the tissue hysteresivity (η), which reflects the coupling of the resistive and elastic properties in the respiratory tissues. The higher frequency components of the real part reflect the airway resistance (Raw), which is the resistance exerted on the flow of gases in the airways. The high-frequency imaginary part represents the airway inertia (Iaw), resulting from the acceleration and deceleration of the oscillating intrapulmonary gas. These considerations can be applied to identify the mechanical properties of the respiratory system by fitting a well-validated mathematical model to the impedance spectra as follows [32]:

$$Z(\omega) = Raw + j{\cdot}\omega{\cdot}Iaw + \frac{G - jH}{\omega^{\alpha}}$$

where Z is the measured impedance, Raw is the airway resistance, ω is the angular frequency ($\omega = 2\pi F$), Iaw is the airway inertance, G is the tissue damping, H is the tissue elastance, $\alpha = (2/\pi)\arctan(H/G)$, j is the imaginary unit.

6. Aims

The general aim of the studies included in the present thesis was to better understand the effects of different anesthetics and pulmonary air and thromboembolism on the respiratory system. Given that the effects of anesthesia protocols commonly used in animal models on lung function have not been systematically compared, the first study aimed to assess the respiratory effects of agents frequently used for general anesthesia, with a specific focus on the following research topics:

I.   To investigate the respiratory effects of five widely used anesthetics in a common rodent model at different positive end-expiratory pressure levels;

II. To measure the responsiveness of the respiratory system under general anesthesia using different anesthetic agents;

III. To compare the mechanical properties and airway responsiveness between the anesthetic regimens used.

In the second study, we aimed to compare changes in indices reflecting airway and respiratory tissue mechanics, gas exchange, and capnography parameters in cases of gas embolism and thromboembolism. The specific aims of this study were:

IV. To measure the changes in lung mechanics, gas exchange, and capnography indices during diffuse gas embolism and focal thromboembolism;

V.   To compare the outcomes of these two different types of lung injury based on the observed parameters.

7. Materials and methods

7.1. Ethical approval

Both experimental protocol was approved by the National Food Chain Safety and Animal Health Directorate of Csongrád County, Hungary (no. XXXII./2110/2019 on December 16, 2019 and no. XXXII./2096/2018 on September 24, 2018). The experimental procedures were performed according to the guidelines of the Scientific Committee of Animal Experimentation of the Hungarian Academy of Sciences (updated Law and Regulations on Animal Protection: 40/2013. [II. 14.], Government of Hungary) and European Union Directive 2010/63/EU on the protection of animals used for scientific purposes. The results were reported according to the ARRIVE guidelines [33].

7.2. Measurement of end-expiratory lung volume
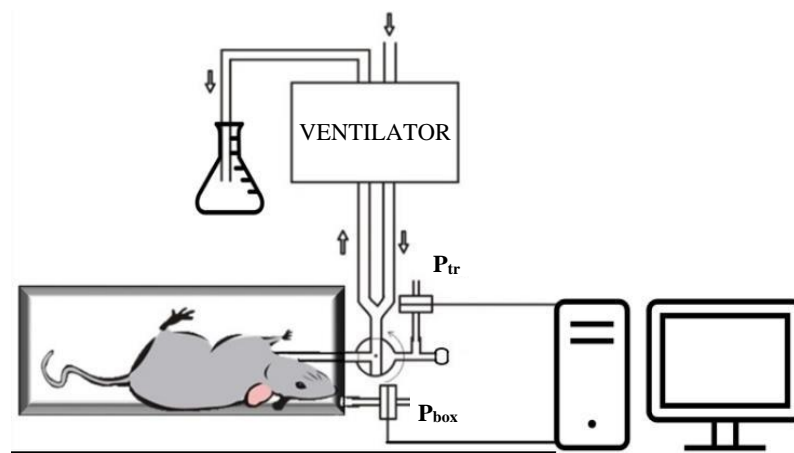
Figure 6 Scheme of the measurement setup for the assessment of thoracic gas volume

Ptr: trachea pressure; Pbox: plethysmography box pressure.

We measured end-expiratory lung volume (EELV) using a custom-made whole body plethysmography box [34]. For these evaluations, the animals were placed in a sealed plexiglas box and ventilated normally.

During measurements, the trachea and box were closed for 10–15 s at end-expiration and pressures inside the box and the trachea were measured during spontaneous breathing efforts of the animal against the closed trachea. Measurements were performed at different levels of positive end-expiratory pressure (PEEP). EELV was calculated from simultaneously measured pressure signals by applying the Boyle–Mariotte law. To compensate for differences in body size between animals, EELV values were normalized to body mass [34].

7.3. Measurement of respiratory mechanics by forced oscillations
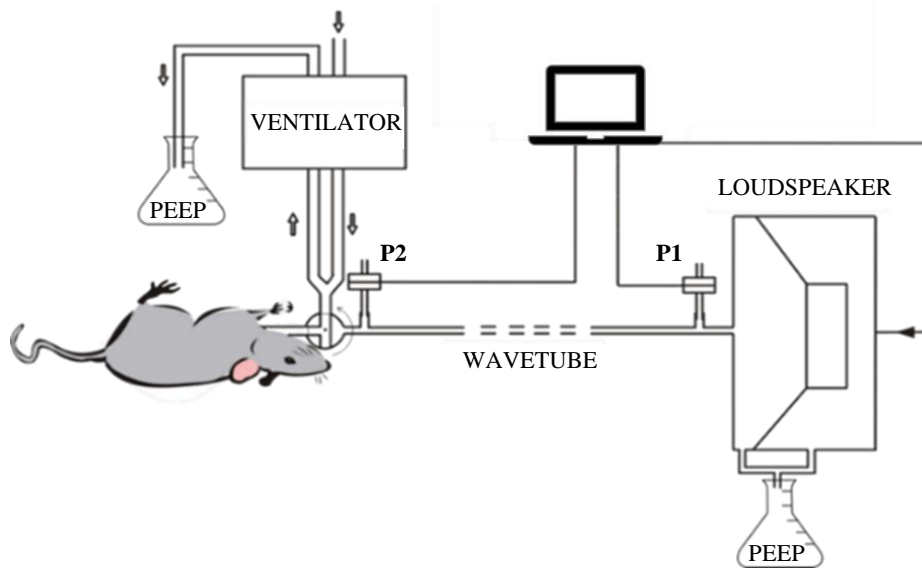
Figure 7 Scheme of the forced oscillatory measurement apparatus

P1 and P2 indicate the pressure sensors at the loudspeaker and at the tracheal end of the wave tube. During the measurements, the respiratory limb was closed, and the animal was connected to the loudspeaker via the wave tube. Between the measurements oscillatory circuit was closed and the respiratory limb was open. To avoid lung derecruitment during the measurements the oscillatory system also needs to be pressurized to the same level of PEEP.

In both studies the mechanical parameters of the airway and respiratory tissues were determined by measuring the input impedance of the whole respiratory system under closed chest conditions (Zrs) or the lung under open chest conditions (Z_L) using the wave-tube approach of the forced oscillation technique [35; 36; 37]. Briefly, a short (8 s) end-expiratory apnea was induced, and the tracheal cannula was connected to a loudspeaker-in-box system by turning a three-way tap. The loudspeaker delivered a small amplitude ($<\pm 1$ cmH$_2$O) pseudorandom forcing pressure signal consisting of 23 non-integer multiples of a 0.25-Hz fundamental frequency between 0.5 and 20.75 Hz through a polyethylene wave-tube (100 cm length, 2 mm internal diameter). Lateral pressures on both ends of the wave-tube were measured (P1 and P2) using two identical differential pressure transducers (24PCEFA6D, Honeywell, Charlotte, NC, USA), low-pass filtered at 25 Hz, and digitized using an analogue-digital converter of a data acquisition board (USB-6211, National Instruments, Austin TX) at a sampling rate of 256 Hz. Pressure transfer functions (P1/P2) were calculated with fast Fourier transformation (4-s time windows and 95% overlapping) from each 6-s recording. Zrs or Z_L

was calculated as the load impedance of the wave-tube from the recordings [38], and at least three consecutive and consistent Zrs or Z_L measurements were ensemble-averaged under each experimental condition. The input impedance of the endotracheal tube and the connections had previously been determined and subsequently subtracted from each Zrs or Z_L spectrum.

A mathematical model was fitted to the Zrs or Z_L spectra by minimizing the relative difference between the measured and modelled impedance data [32]. The model included Raw and Iaw in series with a constant-phase tissue compartment consisting of tissue damping (G) and tissue elastance (H). G describes the dissipative properties (damping and resistance) while H describes the stiffness (elastance) of the respiratory tissues (lung and chest wall). In both conditions, Raw and Iaw describe the flow resistance and inertance of mainly the conducting airways as the contribution of the chest wall is minimal on these parameters [39]. To assess the coupling of elastic and resistive components of the respiratory tissues, η was calculated as G/H.

7.4. Blood gas analyses

Samples of 0.15 ml arterial blood were collected for blood gas analyses, from which the arterial partial pressures of oxygen (PaO_2) and carbon dioxide ($PaCO_2$) were determined using a point-of-care blood analyzer system (Epoc Reader and Host; Epocal, Inc., Ottawa, ON, Canada).

7.5. Recording and analyses of volumetric capnogram

The partial pressure of carbon dioxide (PCO_2) in expired gas and ventilation airflow were simultaneously recorded using a rodent sidestream volumetric capnograph (Harvard Capnograph Type 340 for small rodents) at a sampling frequency of 256 Hz. Volumetric capnogram curves were generated for each expiratory cycle from the PCO_2 tracing and the volume signals obtained by integrating the corresponding ventilation airflow data. The capnogram phase boundaries were determined, and the shape factors were calculated based on previously described concepts [40; 41]. Briefly, the inflection point of phase 2 was determined as the maximum of the first derivative of the volumetric capnogram curve, and the phase 2 slope was measured as the rate of change of PCO_2 around this inflection point. The start and end points of phase 2, which reflect the mixed emptying of airway-alveolar spaces, were identified as the maximum of the third derivative before and after this inflection point in both the time and volumetric domains. The phase 3 capnogram slope, reflecting the dynamics of the alveolar gas compartment emptying, was determined by fitting a linear regression line to the

middle third of phase 3. Normalized phase 2 (Sn2V) and 3 (Sn3V) slopes were calculated by dividing phase 2 and phase 3 slopes by the respective ETCO$_2$ values. This normalization allows a more objective comparison of changes in the capnogram shape due to changes in ETCO$_2$, such as observed in the embolism models used in this study [22; 42; 43].

Volumetric capnography also enables the calculation of Fowler's anatomic dead space (VDF), along with Bohr's physiological dead space (VDB) and Enghoff's modified physiological dead space (VDE). VDF was defined as the exhaled gas volume until the inflection point in phase 2 [44]. VDB was calculated as [45]:

$$\frac{VDB}{VT} = \frac{(PACO_2 - P\bar{E}CO_2)}{PACO_2}$$

where the mean alveolar partial pressure of CO$_2$ (PACO$_2$) was defined as the CO$_2$ concentration at the midpoint of phase 3 in the volumetric capnography curve, and the mixed expired CO$_2$ partial pressure (P$\bar{E}$CO$_2$) was estimated by dividing the integrated capnogram curve by tidal volume (VT) in each expiratory cycle.

VDE, which also comprises nonventilated but perfused alveoli, also known as intrapulmonary shunting, was obtained as follows [46; 47]:

$$\frac{VDE}{VT} = \frac{(PaCO_2 - P\bar{E}CO_2)}{PaCO_2}$$

where PaCO$_2$ is the partial pressure of CO$_2$ in an arterial blood sample.

The alveolar dead space fraction (AVDSf) was also determined [48] as:

$$\frac{PaCO_2 - ETCO_2}{PaCO_2}$$

7.6. Animal preparations

7.6.1. Animal preparations in anesthesia study

Following anesthesia induction, subcutaneous injection of lidocaine (2–4 mg/kg) was locally administered and tracheostomy was performed using a 2.5-mm metal cannula (tracheal cannula with Luer end, 2.5 mm OD, # 732725, Harvard Apparatus, South Natick, MA, USA). Mechanical ventilation was initiated with a rodent ventilator using room air at a VT of 10 ml/kg using a frequency that achieved normocapnia. End-tidal CO$_2$ (ETCO$_2$) was monitored using a

sidestream rodent capnograph (Type 340, Harvard Apparatus, South Natick, MA, USA). The left femoral artery and vein were cannulated using a polyethylene tube (Abbocath 22G). The arterial line was connected to a pressure transducer (MLT0380 Reusable blood pressure Transducer, ADInstruments, Dunedin, New Zealand) and was also used to draw blood samples for arterial blood gas measurements (epoc Reader and Host, Epocal Inc., Ottawa, ON, Canada). The femoral venous line was used for delivery of the anesthetic agent, of pipecuronium a neuromuscular blocking agent at 0.1 mg/kg every 30 min and for administration of the methacholine (MCh) infusion. As a continuous intravenous (iv.) infusion was required for anesthesia maintenance in group PF, an additional venous catheter was inserted into the right jugular vein in the animals of this group. Animals were placed in the supine position on a heating pad with a rectal thermometer connected and set to 37.0°C±0.5°C (Model 507223F, Harvard Apparatus, South Natick, MA, USA). Vital parameters (ECG, arterial blood pressure, body temperature, and exhaled CO_2) were monitored and recorded using a data collection and acquisition system (Powerlab 8/35 and Labchart, ADInstruments, Dunedin, New Zealand).

7.6.2. *Animal preparations in embolism study*

Nine male Wistar rats (362 ± 25 g) were anesthetized by the intraperitoneal (ip.) injection of sodium-pentobarbital (45 mg/kg; Sigma-Aldrich, Budapest, Hungary). The femoral artery and vein were cannulated by 23 G catheters to administer medications, monitor blood pressure, and collect blood samples. Anesthesia was maintained with iv. sodium-pentobarbital (5 mg/kg) every 30 min, and muscle relaxation was obtained by neuromuscular blockade with repeated iv. boluses of pipecuronium (0.2 mg/kg every 30 min; Arduan, Richter-Gedeon, Budapest, Hungary). The body temperature of the rats was maintained at 37°C ± 0.5°C throughout the experiment using a heating pad equipped with a rectal thermometer.

The animals were tracheostomized after local anesthesia with subcutaneous lidocaine (2-4 mg/kg), and the trachea was cannulated with an 18 G uncuffed endotracheal tube. Volume-controlled mechanical ventilation with a VT of 7 ml/kg and PEEP of 5 cmH2O was applied using an identical small animal ventilator. The ventilation frequency was set to 55-60 breaths/min to maintain an ETCO2 level within the normal range (35-45 mmHg). Midline thoracotomy was then performed to access the left pulmonary artery. The mean arterial pressure (MAP) and heart rate were monitored and recorded using the same data collection and acquisition system.

7.7. Study protocols
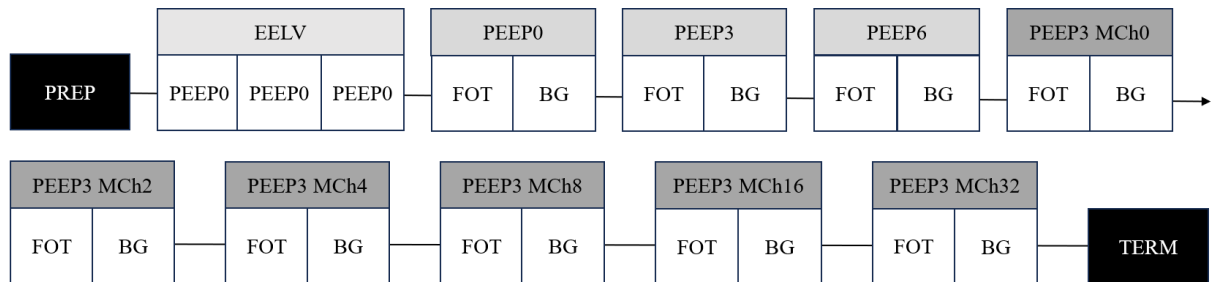
7.7.1. *Study protocol of anesthesia study*

Figure 8 Study protocol of anesthesia study

Schematic of the experimental protocol. PEEP: positive end-expiratory pressure; PREP: anesthesia induction, animal preparation and surgery; EELV: assessment of end-expiratory lung volume; FOT: respiratory mechanical measurements; BG: arterial blood gas sampling; MCh: methacholine challenge; TERM: termination of the animal.

The experimental scheme is illustrated in Figure 8. Following animal preparation, EELV was measured using full body plethysmograph with increasing levels of PEEP at 0, 3 and 6 cmH$_2$O. Animals were then removed from the body box and neuromuscular blockade was initiated. Respiratory mechanics were determined using forced oscillations while maintaining the same PEEP levels as with EELV (0, 3 and 6 cmH$_2$O, again in an increasing order). Arterial blood samples were collected and analyzed at each PEEP level to assess PaO$_2$, partial pressure PaCO$_2$, pH and serum glucose level. Finally, the responsiveness of the respiratory system to an exogeneous bronchoconstrictor stimulus was measured with administration of a continuous iv. infusion of MCh at increasing doses (0, 4, 8, 16 and 32 µg/kg/min) while maintaining a PEEP of 3 cmH$_2$O. Responsiveness to MCh challenge was also assessed by calculating the dose needed for a 100% increase in Raw (ED100$_{Raw}$). All measurements were performed under anesthesia maintained in accordance with group allocation. Animals were euthanized at the end of the experiment using an iv. bolus of 200 mg/kg sodium-pentobarbital.

7.7.2. *Group allocation according to anesthesia induction and maintenance*

In the experiment where we compared the effects of different anesthetics on respiratory mechanics, we performed our measurements on forty male Sprague-Dawley rats (280–540 g, CD® IGS Rat, Charles River, Germany; 8–14 weeks of age). The animals were randomly allocated to one of five experimental groups (N=8 in each group). Groups were assigned according to the anesthetic agent used for induction: group PB were administered an ip. bolus

of sodium pentobarbital (45 mg/kg, [49]), group KX were administered an ip. injection of ketamine (60 mg/kg) and xylazine (10 mg/kg, [49]), group U were administered an ip. injection of urethane (1000 mg/kg, [49]) and groups PF (propofol-fentanyl) and group S were administered inhalational sevoflurane. Those animals were placed in a body box filled with room air and 5% sevoflurane. Inhalational sevoflurane at a concentration of 1 to 2 MAC (2.2%–3.5% [50]) was then continuously administered through a face mask and then using a small animal ventilator (Model 683, Harvard Apparatus, South Natick, MA, USA) through a tracheostomy. Animals were surgically prepared, and anesthesia was maintained according to group allocation. Anesthesia was maintained using repeated iv. boluses of sodium-pentobarbital (12 mg/kg, every 30 min) in group PB [49], applying repeated ip. boluses of ketamine (60 mg/kg) and xylazine (10 mg/kg) every 30 min in group KX [49], using a continuous iv. infusion of propofol 30 mg/kg/h) and fentanyl (5 µg/kg/h) in group PF [49] or continuous inhalation of sevoflurane at a dose of 1-2 MAC (2.2–3.5%, [50]) through a tracheostomy using a ventilator in group S. Additional maintenance of anesthesia following induction was not required in group U [49].

7.7.3. *Study protocol of embolism study*

Following anesthesia induction and surgical preparations, including the thoracotomy, the

Figure 9 Schematic protocol of embolism study

BL: baseline measurements; AE: air embolism; LPAO: left pulmonary artery occlusion;
CAPNO: capnographic measurements; FOT: respiratory mechanical measurements;
BG: arterial blood gas sampling

rats were ventilated as described above with a PEEP of 5 cmH$_2$O throughout the study. After stabilizing vital parameters, a lung recruitment maneuver was performed by closing the expiratory limb of the ventilator tubing until the next expiration to standardize lung volume history. Baseline data were collected 1–2 minutes later by recording capnograph curves and FOT data, along with blood gas analyses of arterial blood samples. Pulmonary air embolism (AE) was then induced by injecting 0.1 ml of air (0.5% of total blood volume) mixed with 0.9 ml of saline into the femoral vein while continuously monitoring the changes in systemic hemodynamics and the capnogram. This injected air volume was titrated in pilot experiments

to exert similar changes in $ETCO_2$ compared to those observed after unilateral pulmonary artery occlusion, yielding comparable gas exchange defects assessed in the expired gas (*see above*). When a peak decrease in $ETCO_2$ was observed (10–15 seconds after the air injection), an additional data set was recorded (condition AE). The effects of AE on systemic hemodynamics and gas exchange parameters lasted approximately 2–4 minutes and then returned to the normal range after approximately 5 minutes, as verified by the continuous monitoring of relevant vital signs. After a 10–15-min stabilization period, the left pulmonary artery was clamped using a small-sized surgical clip, and a third data set, including capnography, forced oscillations, and blood gas analyses, was collected under this condition, i.e. during left pulmonary artery occlusion (LPAO).

7.7.4. *Utility of volumetric capnography in detecting ventilation-perfusion mismatch in models of acute pulmonary embolism – a simulation study*

$$\frac{1}{R_e} = \frac{1}{R_1} + \frac{1}{R_2}$$

$$R_1 = \frac{R_2 \cdot R_e}{R_2 - R_e} \qquad R_2 = \frac{R_2}{R_1} \cdot R_1 = A \cdot R_1$$

$$R_1 = \frac{(A+1) \cdot \text{Re}}{A}$$
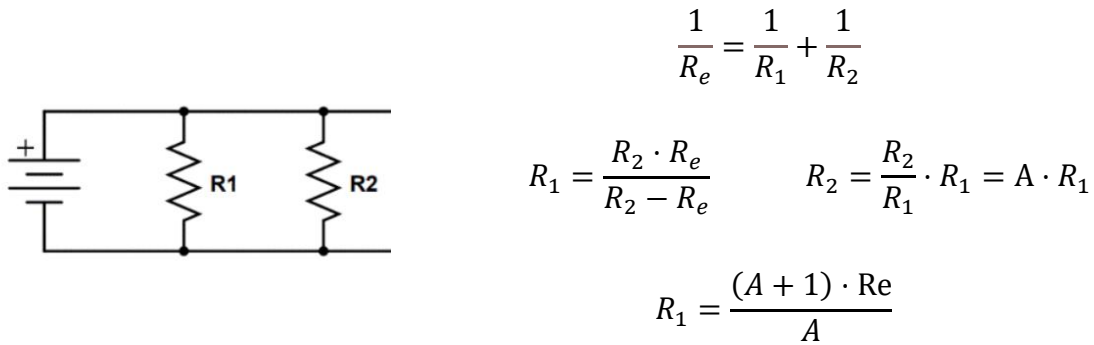
Figure 10 Schematic of wiring diagram and associated equations

R_1: resistance of the lung half with unknown resistance; R_2: resistance of the lung half with known properties; Re: equivalent resistance of the two lung part; A: the split ratio between the two lung halves

A computational study was conducted to model the effects of LPAO on physiological dead space according to Bohr (VDB).

As an initial step, the distribution of VT between the right and left lungs was determined based on a previously reported right-left asymmetrical distribution of 63% versus 37% in rats under physiological conditions [51]. The absolute VT (4 ml), Raw (2 cmH$_2$O.s/l), and VDB (1.43 ml) obtained under control conditions for the whole lung in the present study were distributed between the lung sides according to the previously reported volume asymmetrical distribution.

The mechanical characteristics are corresponding to electrical circuit elements therefore the distribution of VT can be represented with two resistors connected in parallel (Fig. 10)

7.8. Statistical analyses

7.8.1. *Statistical analysis of anesthesia study*

Data are presented as mean $\pm$ SD for normally distributed variables. Normality was checked using the Shapiro-Wilk test. Two-way repeated-measures analyses of variance (ANOVA) with Holm-Šidák post hoc tests were performed to assess the effects of various anesthesia regimes on PEEP-dependence or MCh dose-dependence of respiratory or vital parameters. One-way ANOVA was applied to test for anesthesia-related differences in the responsiveness of the respiratory system. Raw was the primary outcome variable for estimating the sample size required for repeated-measures ANOVA with a power of 0.8 and an alpha of 0.05. Based on previous data [52], the power analysis revealed that at least six animals were required in each protocol group to detect a 40% difference as statistically significant. Two-tailed P-values less than 0.05 were considered statistically significant.

7.8.2. *Statistical analysis of embolism study*

Data are presented as the median with interquartile ranges in each boxplot chart. The Shapiro–Wilk test was used to evaluate the data distributions for normality. For each parameter studied, one-way repeated-measures ANOVA with Holm–Šidák post hoc tests was applied to assess significant differences between the results obtained in the protocol phases. Statistical analyses were performed with the SigmaPlot software package (Version 14, Systat Software, Inc., Chicago, IL, USA). Since changes in lung tissue stiffness were anticipated after embolism, H was considered the primary outcome variable for estimating sample size using one-way repeated-measures ANOVA, with an effect size (f) of 0.4, power of 0.8, and significance level of 0.05. This analysis performed using G*Power (version 3.1.9.7, Universität Düsseldorf, Germany) indicated that at least nine animals were required to detect a 15% significant difference in the primary outcome when considering the previously observed variability [53]. Statistical analyses were performed at a significance level of P<0.05.

8. Results

8.1. Results in anesthesia study

Group KX	Group PB	Group PF	Group S	Group U
405.0 ± 74.4 g	395.6 ± 86.2 g	421.9 ± 56.8 g	420.0 ± 52.4 g	405.0 ± 43.3 g

Table 1 Body masses of the rats in each group.

Data is displayed as mean ± SD. No significant differences were observed. N = 8 in each group. Group KX: group anesthetized with ketamine-xylazine; Group PB: group anesthetized with pentobarbital; Group PF: group anesthetized with propofol; Group S: group anesthetized with sevoflurane; Group U: group anesthetized with urethane
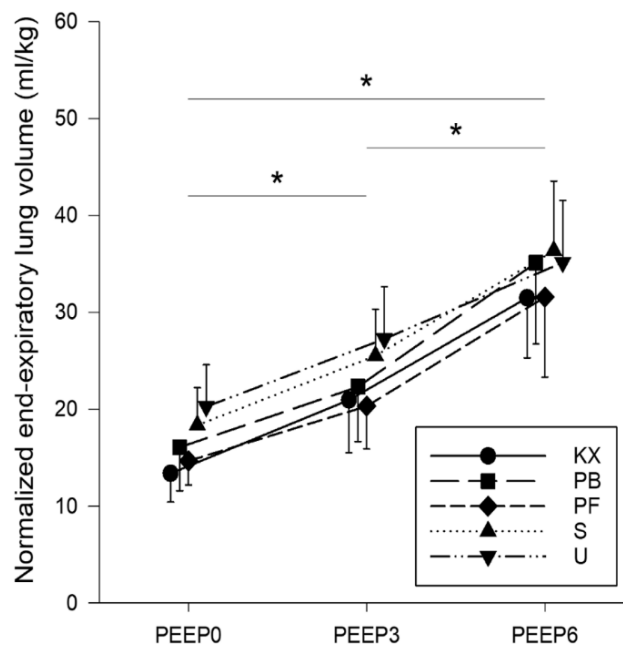
Figure 11 Normalized end-expiratory lung volume (ml/kg)

*End-expiratory lung volumes normalized to body mass. KX, ketamine-xylazine; PB, pentobarbital sodium; PF, propofol-fentanyl; S, sevoflurane; U, urethane; PEEP, positive end-expiratory pressure. *p<0.05 for all groups. N = 8 in each group.*

The body masses of rats are demonstrated in Table 1. No significant differences in body masses were observed between groups (p=0.92). EELV was normalized to body mass due to a wide distribution of body masses within groups. EELV values normalized to body mass are shown in Figure 11. Significant increases in EELV were observed at higher PEEP levels in all

groups (p<0.001 for all), with no differences observed between any of the experimental groups (p>0.10).
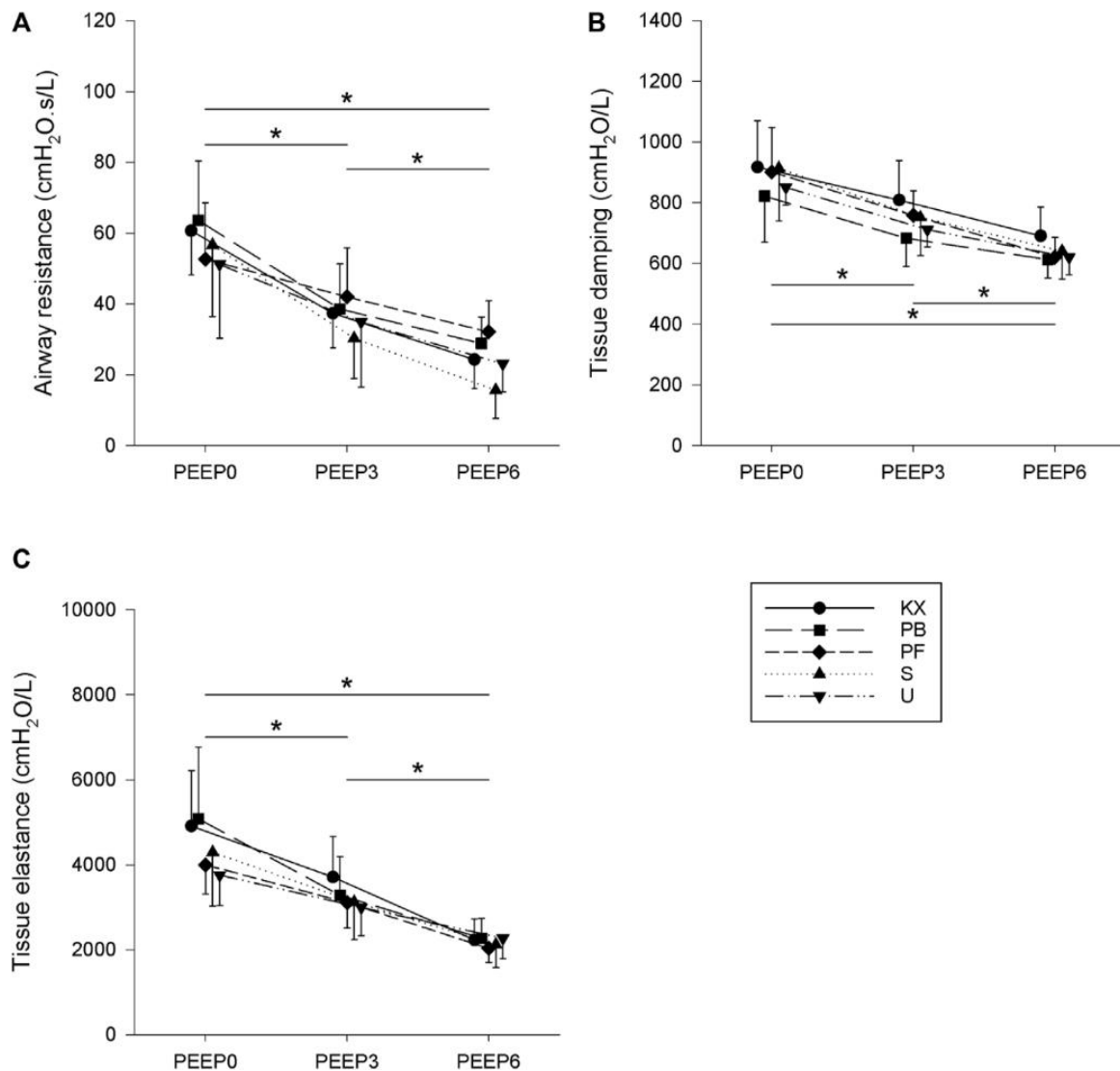
Figure 12 Baseline respiratory mechanical parameters

*(A) Airway resistance. (B) Tissue damping. (C) Tissue elastance. KX, ketamine-xylazine; PB, pentobarbital sodium; PF, propofol-fentanyl; S, sevoflurane; U, urethane; PEEP, positive end-expiratory pressure. *p<0.05 for all groups. N = 8 in each group.*

Baseline respiratory mechanical parameters are illustrated in Figure 12. Raw significantly decreased with increasing PEEP (p<0.001 for all), with no differences observed between any of the experimental groups (p=0.54). Similar trends were observed in terms of the tissue mechanical parameters G and H, with marked effects of PEEP (p<0.001 for all) and no differences between experimental groups (p=0.36 for G and p=0.33 for H).

Figure 13 Baseline blood gas parameters

(A) Partial pressure of O_2 (PaO2). (B) Partial pressure of CO_2 (PaCO2). (C) Arterial pH. (D) Serum glucose. KX, ketamine-xylazine; PB, pentobarbital sodium; PF, propofol-fentanyl; S, sevoflurane; U, urethane; PEEP, positive end-expiratory pressure. *p<0.05 for all groups; #p<0.05 for group KX vs. other groups; †p<0.05 for group U vs. other groups; §p<0.05 for group S vs other groups; % p<0.05 vs. other PEEP levels in group KX. No significant differences in arterial pH values were observed. N = 8 in each group.

Baseline blood gas parameters are depicted in Figure 13. No significant differences in PaO_2 values were observed between groups (p=0.27); however, a negative PEEP-dependence was observed (p<0.001). Increased PEEP caused significant increases in $PaCO_2$ in all groups (p<0.05 in all), with no differences observed between any of the experimental groups (p=0.52). Increasing PEEP levels had no effect on arterial pH (p=0.63), with no differences in arterial pH

values observed between experimental groups (p=0.84). Non-fasting serum glucose levels were not affected by PEEP and were within the normal range in groups PB and PF (p>0.05 in all groups). While PEEP had no significant effect on the serum glucose levels in group S (p>0.50), significantly higher serum glucose levels were observed in group S at a PEEP of 0 cmH_2O compared to groups PB and PF (p=0.03 and p=0.02, respectively). There was a tendency for this difference to be also present at a PEEP of 3 cmH_2O (p=0.06 for PB and p=0.15 for PF), while serum glucose levels in group S did not differ from those in groups PB or PF at a PEEP of 6 cmH_2O (p=0.41 and p=0.61, respectively). Of note, serum glucose levels remained within the normal range for most animals in group S. Conversely, markedly elevated serum glucose levels that exceeded the normal range were observed in groups KX and U, and these values were significantly higher than in all other groups (p<0.001). While PEEP had no effect on the above-normal glucose levels in group U (p>0.05), a significant increase in serum glucose levels with increasing PEEP was observed in group KX (p<0.02).
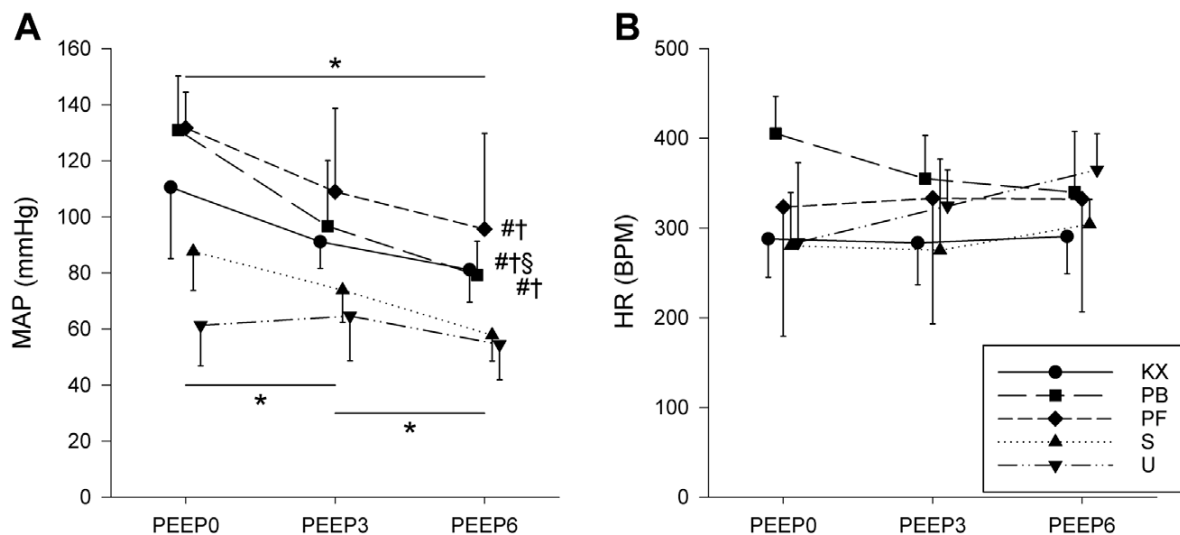
Figure 14 Baseline hemodynamic parameters

*(A) Mean arterial blood pressure (MAP). (B) Heart rate (HR). KX, ketamine-xylazine; PB, pentobarbital sodium; PF, propofol-fentanyl; S, sevoflurane; U, urethane; PEEP, positive end-expiratory pressure. *p<0.05 for all groups; #p<0.05 versus group S; †p<0.05 versus group U; §p<0.05 versus group PF. No significant differences in HR were observed. N = 8 in each group.*

Baseline hemodynamic parameters (MAP and HR) are shown in Figure 14. HR was stable in all groups (p=0.57) regardless of the PEEP applied, with no significant differences between experimental groups (p=0.18). MAP decreased in response to elevated PEEP levels in all groups (p<0.01). Animals in groups S and U had significantly lower MAP values compared to the other

26

three groups (p<0.01). Due to technical difficulties, sufficient hemodynamic data could not be obtained during the MCh provocation.
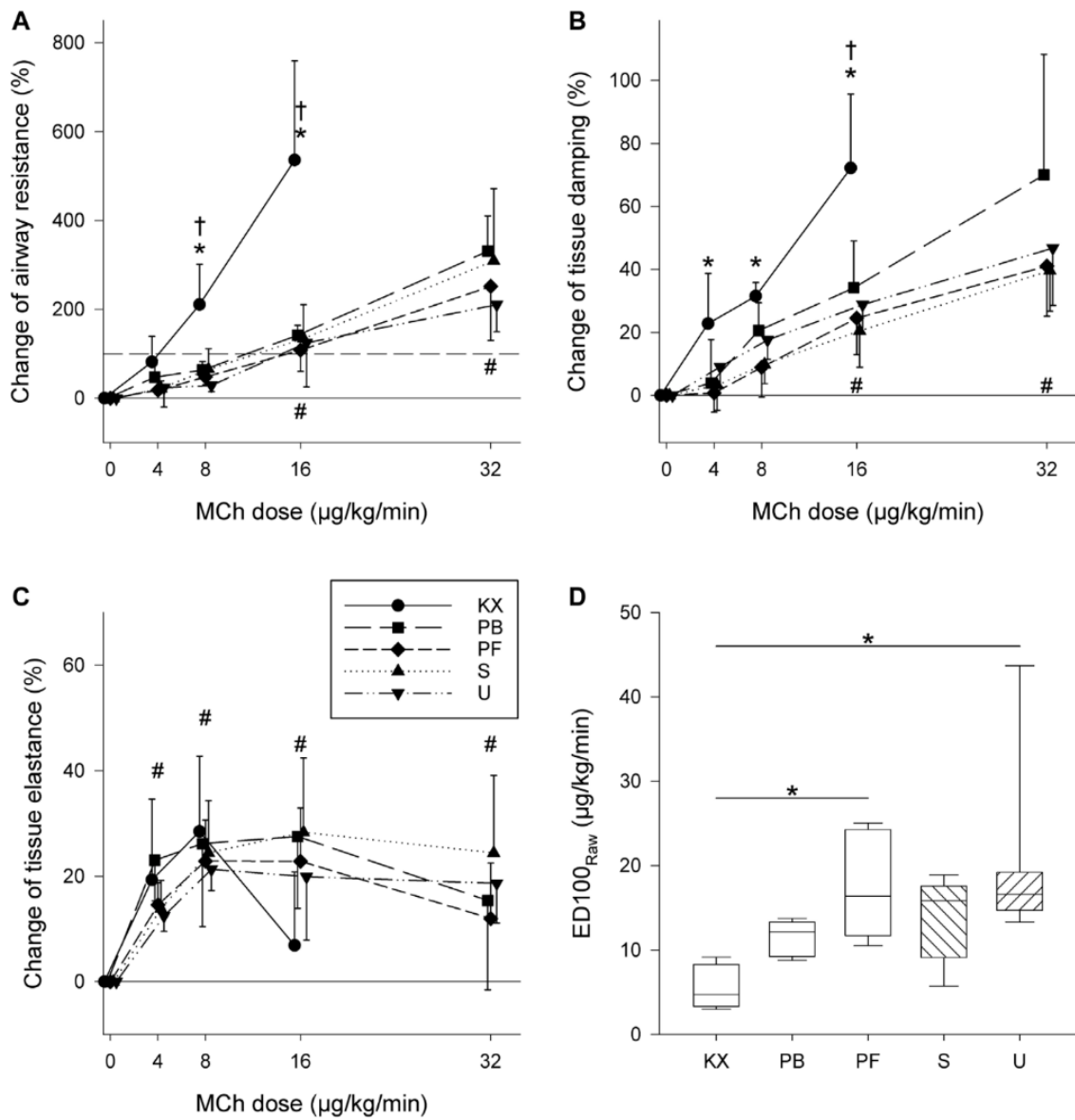
Figure 15 Respiratory mechanics during MCh provocation

(A–C) Changes in respiratory mechanical parameters during intravenous methacholine (MCh) challenge (A) Airway resistance. (B) Tissue damping. (C) Tissue elastance. Solid grey lines indicate baseline values (0 μg/kg/min). Dashed grey lines indicate dose required for a 100% increase in airway resistance. *p < 0.05 vs baseline for group KX; †p < 0.05 Group KX vs. other groups; #p < 0.05 vs. baseline for all groups (D) MCh dose needed to reach 100% elevation of airway resistance (ED100Raw). *: p < 0.05. N = 8 in each group.

Respiratory mechanics during iv. MCh provocation are shown in Figure 15. In terms of Raw, group KX exhibited increased reactivity compared to the other groups, with statistically significant increases observed at 8 and 16 μg/kg/min compared to baseline. Accordingly, the highest increases in Raw were in group KX compared to other groups (p<0.001). Due to severe bronchoconstriction (535%±223% increase compared to baseline), MCh provocation was aborted in all animals in group KX at 16 μg/kg/min instead of 32 μg/kg/min in other groups. In all other groups, significant elevations in Raw were observed during MCh infusion rates of 16 and 32 μg/kg/min compared to baseline. This difference in airway reactivity was also reflected in the average values of ED100$_{Raw}$, with the lowest ED100$_{Raw}$ values observed in group KX (p<0.03).
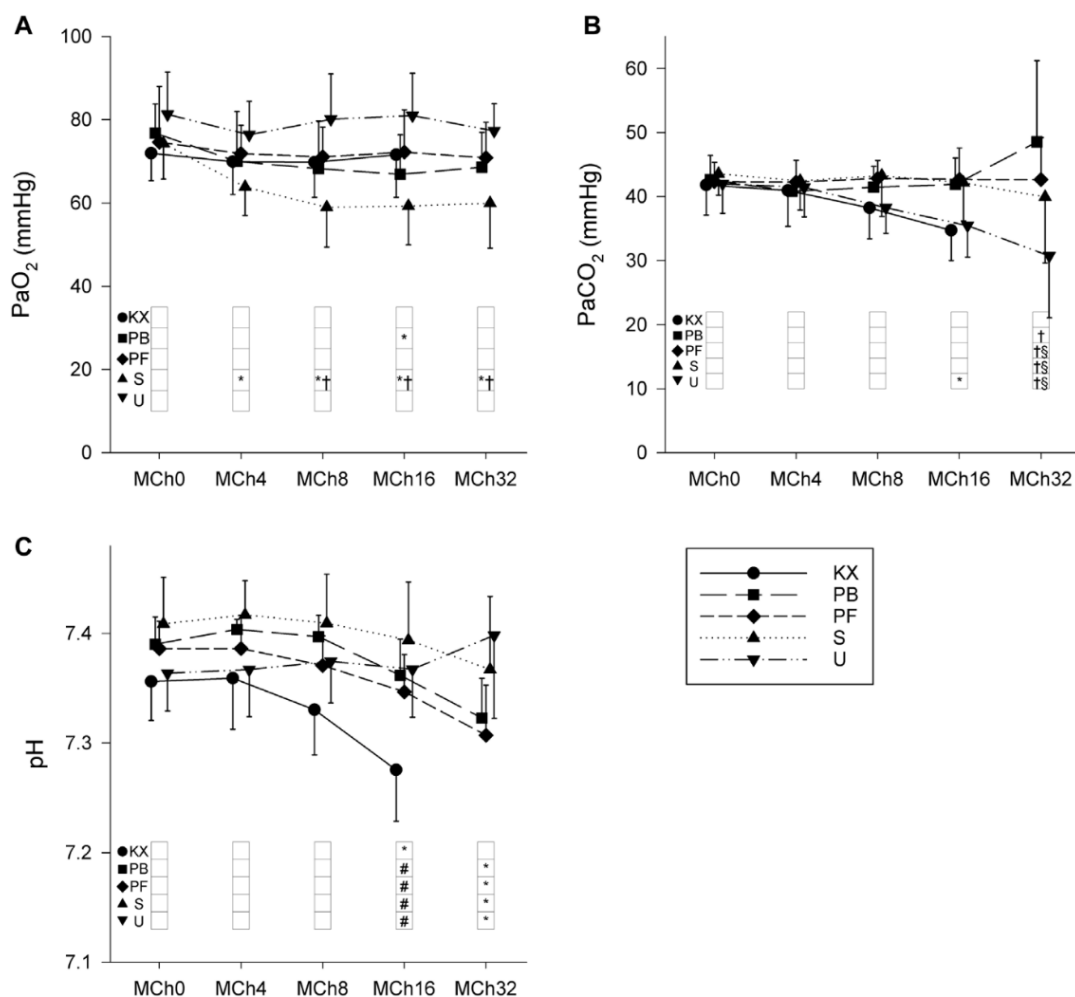
Figure 16 Changes in arterial blood gas parameters during intravenous MCh challenge

(A) Partial pressure of O_2 (PaO$_2$). (B) Partial pressure of CO_2 (PaCO$_2$). (C) Arterial pH. KX, ketamine-xylazine; PB, pentobarbital sodium; PF, propofol-fentanyl; S, sevoflurane; U, urethane. *p < 0.05 vs. MCh0; #p < 0.05 vs. Group KX; †p < 0.05 vs. Group U; §p < 0.05 vs. Group PB. N = 8 in each group.

28

Significant elevations of G were also observed in group KX at MCh infusions at 4 μg/kg/min and above compared to baseline (p<0.001). No differences were observed in G between the other experimental groups (p>0.29), with significantly higher G values observed at MCh infusions of 16 and 32 μg/kg/min (p<0.001). In terms of H, no significant differences were observed between experimental groups (p=0.80), with significant elevations observed starting at MCh infusion rates 4 μg/kg/min and above (p<0.001).

Changes in blood gas parameters during iv. MCh provocation are shown in Figure 16. MCh administration had no effect on PaO_2 in most groups; however, lower PaO_2 values were observed in group S (p<0.01). Similar trends were observed with $PaCO_2$ values, with decreased $PaCO_2$ values observed in group U at the two highest doses of MCh (p<0.04). Significant difference in arterial pH were observed at the highest dose of MCh compared to baseline in all groups (p<0.04) with the exception of group U (p=0.7). Despite the differences in these trends, no between-group differences were observed at any of the MCh infusion rates used.

8.2. Results in embolism study
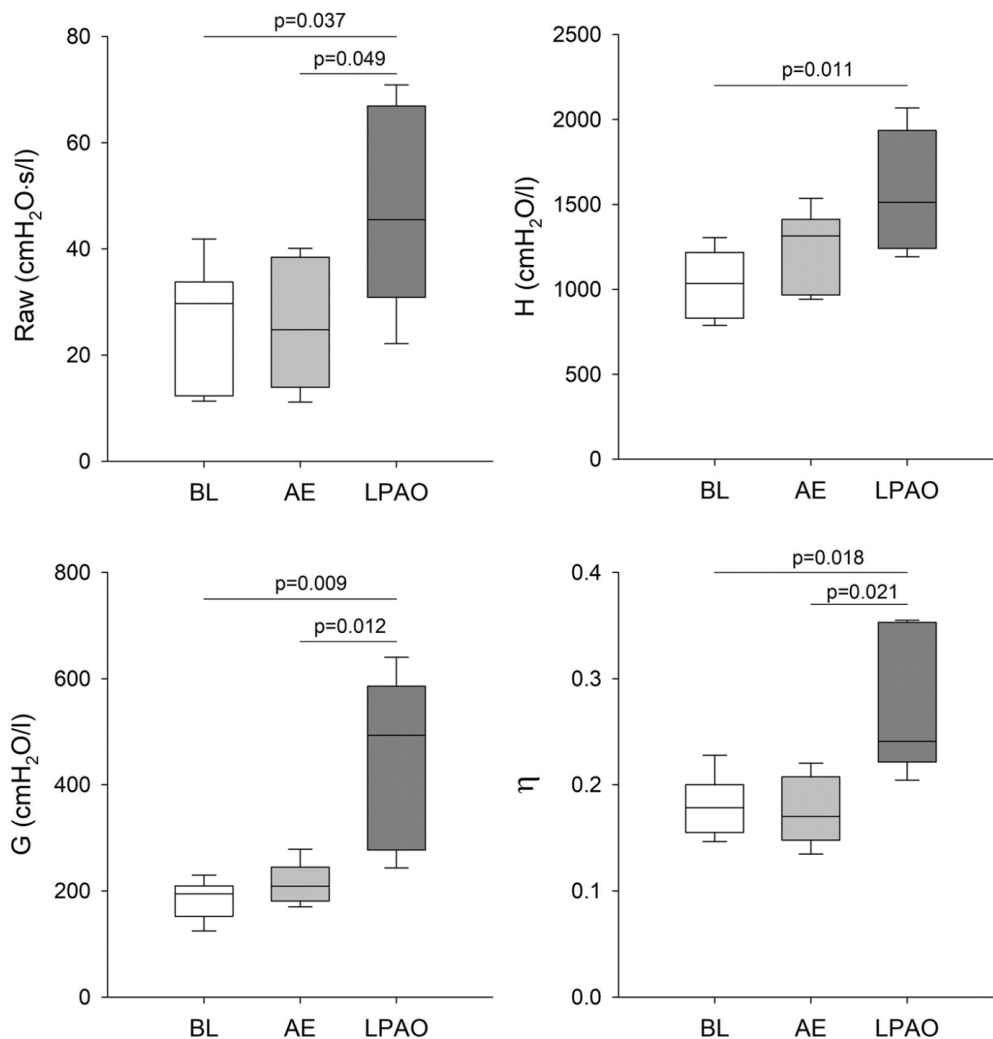
Figure 17 Mechanical parameters in embolism study

Airway and respiratory tissue mechanical parameters at baseline (BL),
following air embolism (AE), and after left pulmonary artery occlusion (LPAO).
Raw: airway resistance, H: tissue elastance, G: tissue damping, η: tissue
hysteresivity (defined as G/H)

The mechanical parameters of the respiratory system under baseline conditions and following induction of pulmonary embolism by two different mechanisms are shown in Figure 17. No significant changes in these parameters were observed after AE. In contrast, significant increases in all parameters reflecting airway (Raw) and respiratory tissue mechanics (H, G, and η) were obtained after clamping the left pulmonary artery compared to baseline values ($p < 0.05$ for all). Significant differences in Raw, G, and η were observed between the

two forms of embolism (p<0.05 for all), while there was a trend toward a significant difference in H (p=0.1).
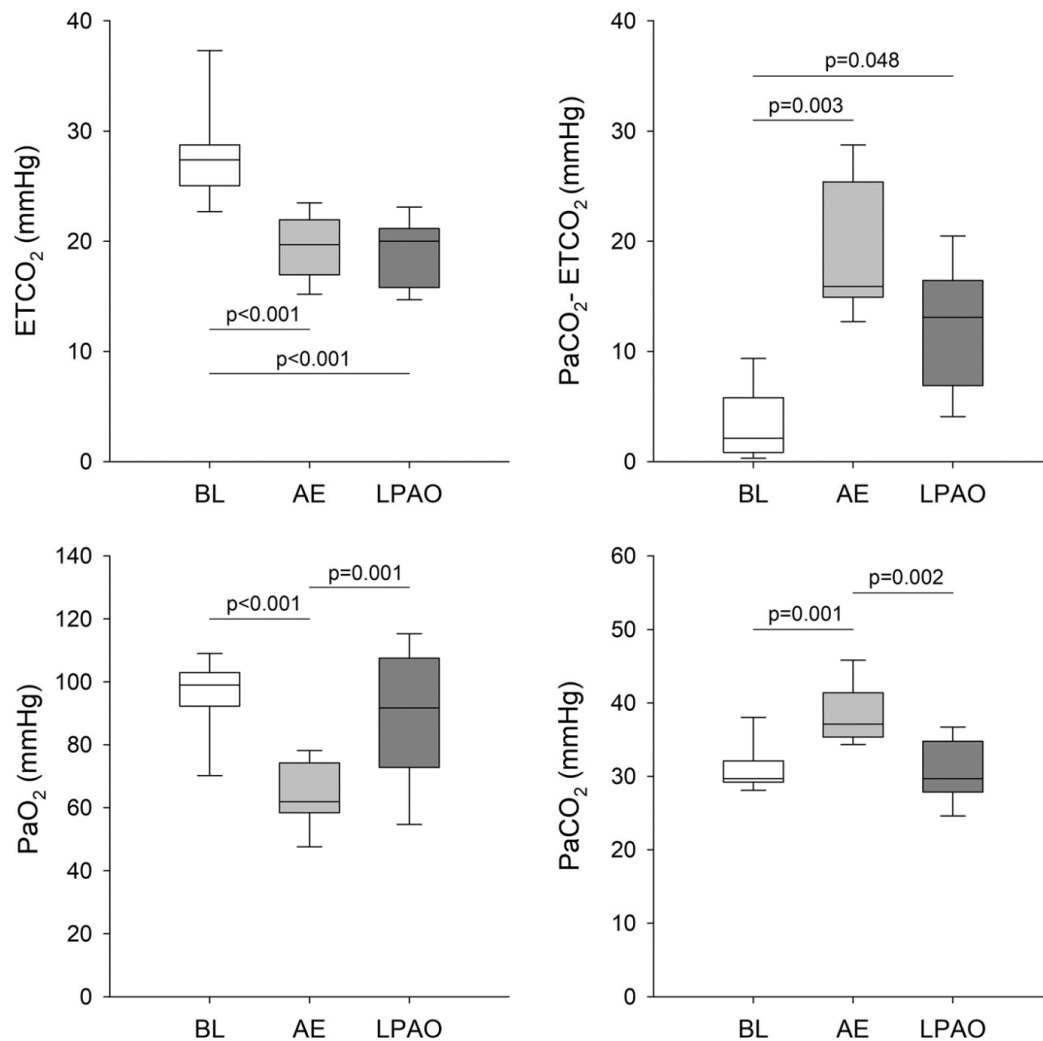
Figure 18 Blood gas parameters

Arterial blood gas parameters and related capnogram indices obtained at baseline (BL), following air embolism (AE), and after left pulmonary artery occlusion (LPAO). ETCO$_2$: end-tidal carbon dioxide, PaCO$_2$-ETCO$_2$: arterial to the end-tidal CO$_2$ pressure gradient, PaO$_2$: arterial partial pressure of oxygen, PaCO$_2$: arterial partial pressure of carbon dioxide

Figure 18 summarizes ETCO$_2$, the PaCO$_2$-ETCO$_2$ gradient, and the arterial blood gas parameters under the baseline condition and following the induction of embolism by the two different mechanisms. In accordance with our experimental approach to induce comparable gas exchange defects assessed in the expired CO$_2$ concentration, the significant decreases in ETCO$_2$ did not differ between the two embolism models (p<0.001 vs. baseline for both). Furthermore, increases in PaO$_2$-ETCO$_2$ of comparable magnitude were observed in both embolism models

(p<0.05 vs. baseline for both). A significant decrease in PaO_2 and a significant increase in $PaCO_2$ were observed following AE (p<0.001 for both). However, these parameters were not significantly affected by LPAO, resulting in significant differences in PaO_2 and $PaCO_2$ between the two forms of pulmonary embolism (p<0.001 for both). There was a strong tendency for an increase in the arterial lactate level, with increasing from the baseline value of 2.6±0.8 mmol/l to 3.6±1.3 and 4.3±1.8 mmol/l after AE and LPAO, respectively (p=0.056).
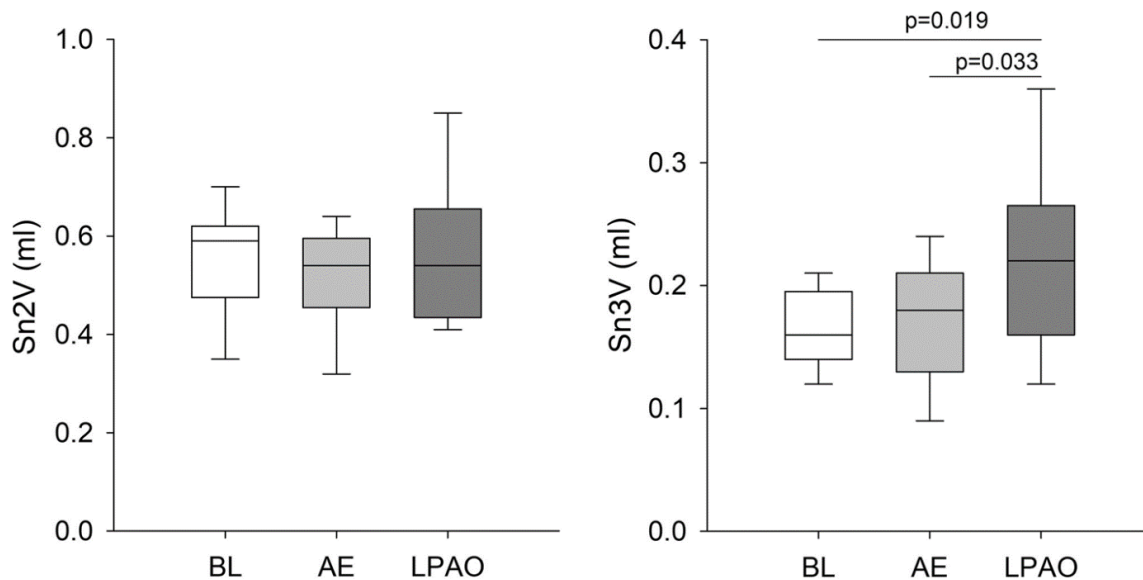
Figure 19 Shape factors

Phase 2 and 3 slopes of the volumetric capnogram normalized to the end-tidal CO_2 concentration obtained at baseline (BL), following air embolism (AE), and after left pulmonary artery occlusion (LPAO)

Figure 19 shows shape factors representing the normalized phase 2 and phase 3 slopes obtained by volumetric capnography. No significant change in Sn2V was observed after either form of embolism. In contrast, significant increases in Sn3V were evidenced following LPAO compared to baseline and after AE (P<0.05 for both).

Changes in dead space indices at different protocol stages are shown in Figure 20. There were no significant changes in VDF or VDB following either form of embolism. However, a significant increase in the VDE dead space fraction was observed following AE and LPAO (P=0.003 and P<0.05, respectively). A significant increase in AVDSf compared to the baseline condition was also observed following both forms of embolism (P<0.001 for both), with a trend toward increased AVDSf following AE compared to LPAO (P=0.063).
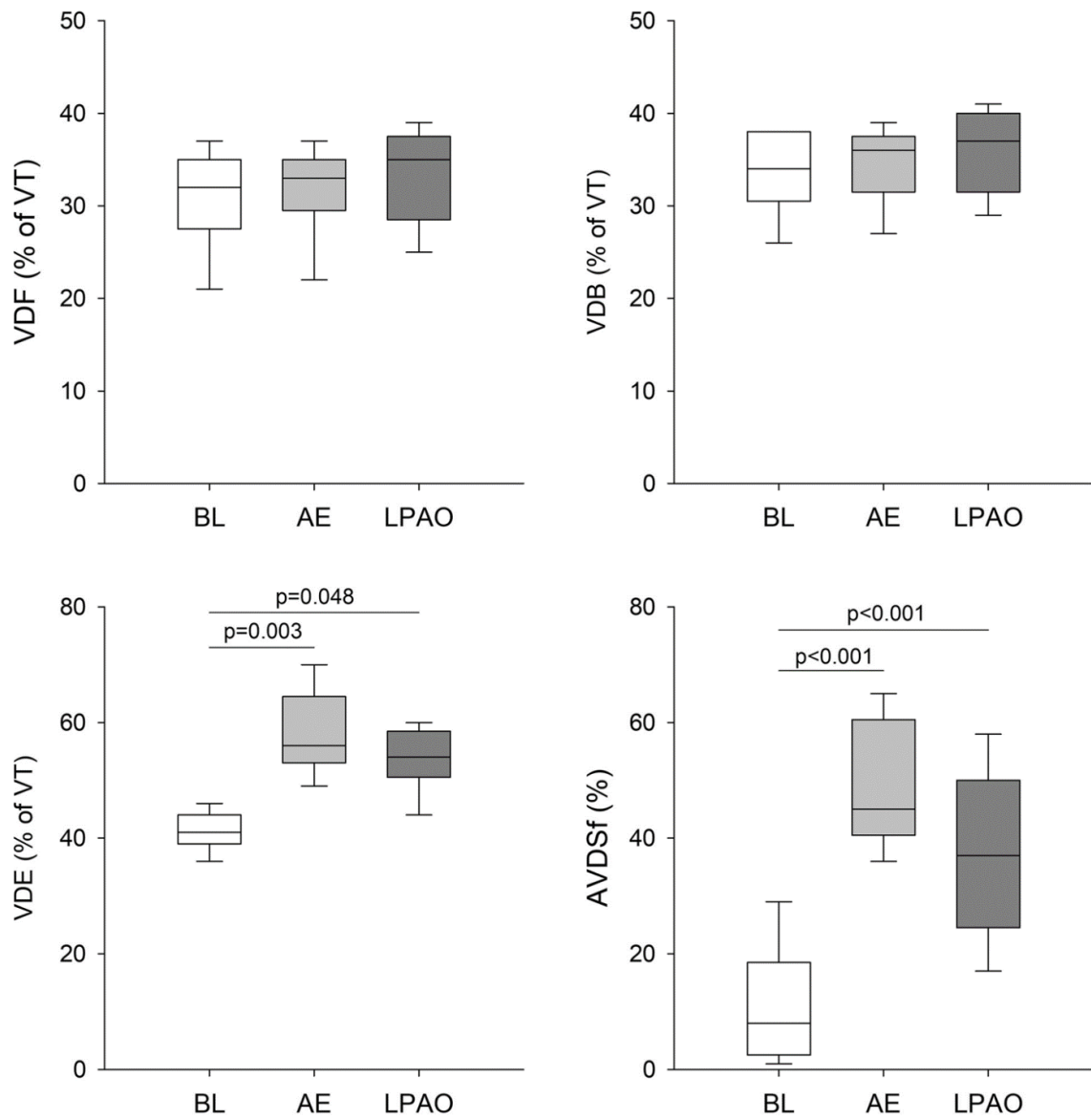
Figure 20 Dead space indices

Fowler anatomical (VDF), Bohr (VDB), and Enghoff (VDE) physiological dead spaces, and alveolar dead space fraction (AVDSf) expressed as a percentage of tidal volume (% of VT) obtained at baseline (BL), following air embolism (AE), and after left pulmonary artery occlusion (LPAO)

	Before AE	AE	2 mins after AE	Before LPAO	LPAO	2 mins after LPAO
MAP (mmHg)	116 ± 11	$64 \pm 21^{*}$	110 ± 9	125 ± 4	$30 \pm 10^{*\#}$	108 ± 12
HR (BPM)	490 ± 57	$352 \pm 48^{*}$	474 ± 69	473 ± 24	$215 \pm 46^{*\$}$	463 ± 24

Table 2 Hemodynamics before, during and after embolism

*Mean arterial pressure (MAP) and heart rate (HR) expressed as mean ± SD obtained before air embolism (Before AE), at the peak response following AE, and 2 minutes later. Values are also reported immediately before the left pulmonary artery occlusion (LPAO), at the peak response after LPAO, and 2 minutes after release of the left pulmonary artery.*
*: p<0.001 vs. BL, #: p<0.001 vs. AE, \$: p=0.013 vs. AE

Table 2 demonstrates the changes in the systemic hemodynamics before, during, and after the embolic insults. AE and LPAO induced significant transient decreases in MAP and HR (p<0.001, for all). Complete recoveries of MAP and HR were observed after AE with no significant difference compared to the values obtained before the interventions.

8.3. Results of the simulation study

	Control condition			LPAO		
	Right lung	Left lung	Whole lung	Right lung	Left lung	Whole lung
Volume ratio (%)	63	37	**100**	83	17	**100**
VT (ml)	2.52	1.48	**4.00**	3.33	0.67	**4.00**
Raw (cmH$_2$O.s/l)	47.3	57.8	**26**	57.8	289.2	**48.2**
VDB (ml)	0.90	0.53	**1.43**	0.95	0.53	**1.48**
VDB (% of VT)	35.7	35.8	**35.8**	28	80	**37**

Table 3 Results of the computational simulation study.

LPAO: left pulmonary arterial occlusion; Volume ratio: lung volume distribution in the two lungs; VT: tidal volume; Raw: airway resistance; VDB (ml): anatomic dead space according to Bohr; VDB (% of VT): dead space ratio normalized to VT

Following LPAO, severe hypocapnia developed in the occluded left lung resulting in a marked bronchoconstriction. Based on previous studies, Raw is increased by approximately 5-6-fold in the occluded lung, i.e. Raw rises from 57.8 to 289.2 $cmH_2O.s/l$ [54]. Kirchhoff's Law for parallel circuits can be used to assess the Raw in the contralateral right lung once the overall Raw is known to have increased from 26 to 48.2 $cmH_2O.s/l$ following LPAO. As the distribution of VT between the right and left lungs is governed by the lateral Raw in the absence of marked asymmetry in the tissue mechanics [54], VTs of 3.33 and 0.67 ml were observed in the right and left lungs, respectively. The total VDB of 1.48 ml obtained in our experiments after LPAO was then distributed between the two lungs by assuming that perfusion of the left lung was almost entirely absent, with only a small proportion (20%) of normal perfusion maintained due to preserved systemic bronchial circulation or incomplete blockade of the left pulmonary artery. This resulted in a VDB of 0.53 ml for the occluded left lung (80% of VT reaching the left lung) and 0.95 ml for the right lung (28% of VT reaching the right lung).

9. Discussion

The results of the studies included in the present thesis demonstrated changes in the respiratory system in two different translational animal models.

The mechanical properties of the airways and the respiratory tissues are of critical importance in determining gas exchange. The respiratory mechanics is affected by a wide variety pulmonary disorders and diseases (e.g. COPD, asthma, pulmonary embolism) and medical interventions (e.g. various drugs, mechanical ventilation, general anesthesia). Although the pharmacological effects of the various anesthetic agents have been studied excessively, there is still a lack of knowledge of how they affect respiratory mechanics. Thus, we focused our first investigation on how sodium-pentobarbital, ketamine-xylazine, propofol-fentanyl, sevoflurane and urethane affect various properties of the respiratory system and we also assessed their modulation potential in response to bronchoprovocation.

Furthermore, pulmonary embolism is a common and potentially life-threatening condition. One of the quick and accurate diagnostic tools of embolism is the characteristic distortion of the capnogram curve. With regard to the type of embolism, different changes in the capnogram curve and respiratory mechanics can be observed when the pulmonary ischemia is subsequent to air bubble or a thrombus. Therefore, in our second study we aimed to compare these changes in translational models of air- and thromboembolism.

9.1. Effects of general anesthesia

In this study we aimed to characterize the respiratory effects of iv. sodium-pentobarbital, iv. propofol-fentanyl, ip. ketamine-xylazine, inhaled sevoflurane and ip. urethane, which are all commonly used anesthesia regimes in rats. No significant differences in lung volume, baseline respiratory mechanics or blood gas parameters were observed between the anesthesia regimes at three different levels of PEEP. On the contrary, significant bronchial hyperreactivity was observed with the administration of increasing doses of iv. MCh in rats undergoing ketamine-xylazine anesthesia. Respiratory parameters in all groups were in good agreement with data acquired previously by us in healthy animals in the same mass range and rats undergoing pentobarbital anesthesia [52; 55].

9.1.1. Effects of general anesthesia on baseline respiratory mechanics

The lack of differences in baseline respiratory mechanical parameters between experimental groups in this study may be attributable to a number of reasons. General anesthesia induces respiratory depression with practically all anesthetic agents to various extents [5; 6; 7], and such

effects are particularly evident with the use of pentobarbital [56; 57] and propofol [58]. However, all animals were mechanically ventilated in this study, which prevented lung volume loss and subsequently contributed to the similar EELV values observed between experimental groups. This feature of this study in addition to physiologically low basal airway smooth muscle tone can explain the lack of the previously described bronchodilator effects of sevoflurane [10] and propofol [59]. While the bronchodilator effect of sevoflurane has been consistently reported in subjects with increased bronchial tone (e.g. asthma [60], chronic obstructive pulmonary disease [61] and following cardiopulmonary bypass [10]), the bronchodilator effect of sevoflurane in normal subjects remains controversial [11; 12; 62]. Similar to our findings, no bronchoactive properties of propofol [63] or sevoflurane [9; 64] were demonstrated under baseline conditions in a previous study, with propofol found to have no bronchoprotective effect against bronchoconstrictive agonists [63; 65].

9.1.2. *Effects of general anesthesia on the responsiveness of the respiratory system*

In contrast to previous findings under baseline conditions, anesthesia regimes can significantly affect respiratory function during MCh-induced bronchoconstriction. Significant increases in Raw during ketamine-xylazine anesthesia demonstrated severe bronchial hyperreactivity compared to all other anesthetic regimes. The mechanism underlying this hyperreactivity remains unclear. Ketamine acts against cholinergic bronchoconstriction in isolated human [66] and guinea pig bronchi [67; 68], and sensitized rats [69] and sheep [63] *in vivo*. Previous studies on the bronchial effects of xylazine are limited; however, almost all describe a bronchodilatative effect of xylazine through activation of bronchial alpha-2 receptors [70]. The discrepancy between the previously described bronchial effects of these two anesthetics when used in isolation and our results with the combined administration of ketamine and xylazine indicates that the combination of the two drugs may result in increased airway reactivity. This increased Raw was also coupled with increased G and decreased arterial pH. While Raw is considered a measure of flow resistance in central conducting airways [39], G has more contributing factors. Elevation of G can most prominently indicate ventilation heterogeneity due to inhomogeneous small airway constriction and/or closure [32; 71]. As ketamine reportedly increases the collapsibility of the lung periphery, subsequent increases in ventilation heterogeneity may explain substantial increases in G [72]. While the protective effects of volatile anesthetics (including sevoflurane) against cholinergic bronchoconstriction are well-established [9; 10; 11; 12], we were unable to demonstrate a protective effect of sevoflurane on bronchoconstriction in this study. This finding may be attributable to the

sustained bronchoconstriction and prolonged administration of sevoflurane in our study protocol. Indeed, sevoflurane has previously been shown to reverse cholinergic bronchoconstriction only transiently with a short duration of effect (approximately 5 min.) [73].

9.1.3. Effects of general anesthesia on blood sugar levels

Apart from the respiratory effects of the applied anesthetics, their applicability and other vital parameters also warrant discussion. Non-fasting serum glucose values were within the normal range in animals under pentobarbital, propofol-fentanyl or sevoflurane anesthesia. However, blood sugar values above the normal range were observed under urethane and ketamine-xylazine anesthesia. Urethane-induced hyperglycemia may be mediated by increased sympathetic activation via alpha-2 receptors [74; 75; 76]. The progressive hyperglycemia observed in group KX has previously been observed in studies using ketamine [77; 78] or xylazine [79] alone and in combination [80]. This finding may also be attributable to an alpha-2 receptor-mediated response, resulting in inhibition of insulin secretion [77; 80].

9.1.4. Effects of general anesthesia on systemic hemodynamics

Normal MAP values and HR were observed in all groups, with the lowest MAP values (approximately 60 mmHg) observed in animals under sevoflurane and urethane anesthesia. This finding is in concordance with the results of previous studies describing the hemodynamic effects of these anesthetic agents [81; 82; 83; 84; 85; 86; 87].

9.1.5. Effects on general anesthesia on other organ systems

Our findings on the effects of anesthetic agents on pulmonary system can also be considered in the context of their generalized potential to influence the function of various other organ systems. Tendency for neuroprotection was proposed for volatile agents, such as sevoflurane against neuronal injury in rats [88; 89], barbiturates like pentobarbital [90; 91], propofol [91] and ketamine [92]. Conversely, the neurological effects of urethane are different compared to other anesthetics without a major effect on the peripheral nervous system and various subcortical areas [93], thereby allowing the induction of various peripheral reflexes or characterizing cerebral processes like natural sleep [94]. This characteristic of urethane also results in a lesser amount of respiratory depression in spontaneously breathing animals without inducing apneic periods observed with other anesthetics [94]. Related to the effects of short-term general anesthesia on the liver, various studies have described either dose-dependent or idiosyncratic hepatotoxicity after using sevoflurane [95] or propofol [96], but not with most barbiturates used for sedation or anesthesia, or ketamine [97]. These hepatotoxic effects need

however, a longer timeframe to develop. It is important to note the carcinogenic effects described with urethane, resulting in the development of both benignant and malignant tumors in various organs of the animals, especially after repeated injections [98; 99]. Thus, it is not recommended to use urethane anesthesia in surviving animals [49].

9.1.6. *Considerations with depth of anesthesia*

Regarding the depth of anesthesia, no signs of inadequate anesthesia or inconsistency in the plane of anesthesia were observed in any of the experimental groups, as confirmed by the stability of HR and blood pressure in similar experimental conditions and also before and after the administration of boluses where applicable. The depth of anesthesia was also comparable between the different study groups, as the vital parameters of the animals were comparable with differences explainable by the known effects of the various regimes. Of note, the onset of anesthesia was extremely long in group U (approximately one hour), and while the dose was determined based on previous studies and published best practices, half of the animals (N=4) required an additional injection of approximately 50% of the dose administered before baseline measurements.

9.2. Effects of pulmonary embolism

This study revealed fundamental differences between models of pulmonary embolism, although comparable decreases in the expired carbon dioxide concentration were induced by the gas- and thromboembolic models. Unilateral pulmonary arterial occlusion caused marked elevations in the bronchial tone and compromised lung tissue mechanics, whereas AE did not affect lung mechanics. In contrast with these lung mechanical changes, AE was the only insult that caused significant deteriorations in the arterial blood gas parameters, while partial pressures of oxygen and carbon dioxide in the arterial blood were unaffected by LPAO. No changes VDF or VDB reflecting ventilated but poorly perfused lung areas were observed in either embolism model. Conversely, both AE and unilateral pulmonary artery occlusion resulted in elevated alveolar dead space indices that indicate intrapulmonary shunting (Enghoff and AVDSf).

9.2.1. *Airway mechanical effects of pulmonary embolism*

The main finding of this study was that distinct lung mechanical responses developed in response to the different models of lung embolism, even in the presence of similarly deteriorated $ETCO_2$ levels. In contrast to the lack of changes in lung mechanics following AE, marked bronchoconstriction developed in response to LPAO (Fig. 17). This finding can be

explained by the ability of the CO_2 content of the intrapulmonary gas to modulate the airway smooth muscle tone, resulting in severe bronchospasm below a threshold partial pressure of CO_2 of approximately 10 mmHg [54] Reaching this threshold CO_2 concentration in the ischemic left lung during LPAO explains the elevations in Raw. The magnitude of the overall increase in the Raw was blunted by the intact right lung, which was probably somewhat overinflated. Conversely, the diffuse pulmonary hypoperfusion that developed after AE was likely to cause a moderate and relatively evenly distributed hypocapnia in the bronchoalveolar system, in which the threshold concentration to trigger a bronchial smooth muscle contraction was not reached [54].

9.2.2. Lung tissue mechanical effects of pulmonary embolism

These differences in the airway responses between AE and LPAO were associated with distinct changes in the forced oscillatory parameters reflecting respiratory G and stiffness (H). The excessive increase in G over those in H indicates the development of ventilation heterogeneities *[100]*. As this pattern of change was observed only after LPAO, the impairment in respiratory tissue mechanics indicates that considerable ventilation inhomogeneity developed after LPAO due to uneven lung ventilation resulting from the additive effects of volume loss in the left lung and overdistension of the right lung. The presence of this phenomenon was confirmed by the elevations in mechanical and capnography parameters sensitive to ventilation heterogeneities (η and Sn3V).

9.2.3. Effects of pulmonary embolism on blood gas parameters

Changes in blood gas parameters notably differed between the two embolism models, with significant deteriorations observed only after a diffuse pulmonary perfusion defect generated by AE (Fig. 18). In agreement with previous findings [101; 102; 103], acute AE led to the development of hypoxia and hypercapnia. The adverse gas exchange defects were reflected in the alveolo-end-tidal CO_2 gradient (Fig. 18) and in the marked elevations in VDE and AVDSf (Fig. 20). Since VDE and AVDSf incorporate poorly ventilated but perfused alveoli with low ventilation-perfusion matching [104], increased intrapulmonary shunting may be responsible for this finding as a consequence of a perfusion redistribution [103]. Interestingly, blood gas parameters were unaffected by LPAO despite concomitant increases in capnography parameters reflecting intrapulmonary low ventilation-perfusion perfusion areas and shunting ($PaCO_2$-$ETCO_2$ in Fig. 18 and VDE and AVDSf in Fig. 20) and in the airway and respiratory tissue mechanics (Fig. 17). The absence of changes in PaO_2 following LPAO agrees with

40

previous results demonstrating that oxygenation can remain normal following acute pulmonary thromboembolism [105; 106]. This finding is likely attributable to the unaffected right lung being able to maintain blood gas parameters within the normal range due to increased VT in response to hypocapnic bronchoconstriction in the ischemic left lung [107].

9.2.4. Effects of pulmonary embolism on anatomical dead space

No change in VDF was observed after inducing lung embolism using air bubbles or unilateral pulmonary vascular ischemia (Fig. 20). As VDF reflects the amount of gas in the conducting airways [44], this finding demonstrates that there was no change in the anatomical dead space fraction following either intervention. While severe bronchoconstriction in the hypocapnic left lung may yield a unilateral reduction in apparent anatomic dead space [108], the redistribution of VT to the right lung may have overinflated this compartment, thereby counterbalancing the anatomic dead space.

9.2.5. Effects of pulmonary embolism on physiological dead space

The lack of change in VDB after either form of embolism is worth noting (Fig. 20). Unilateral occlusion of the pulmonary artery is expected to result in nonperfused but well-ventilated lung regions. Furthermore, the development of a similar ventilation-perfusion mismatch is expected after introducing air into the pulmonary circulation. Accordingly, elevations in VDB can be anticipated in both models of embolism based on Riley's 3-compartment lung model, in which VDB reflects the amount of well-ventilated but poorly perfused alveolar compartments [109]. This seemingly controversial result can be explained by the complex pathophysiological processes initiated by the massive ventilation-perfusion mismatch after embolism. Development of severe bronchoconstriction in the hypocapnic left lung following LPAO can reach a degree where airflow redistribution from the left into the right lung results in a constant VDB. The presence of this mechanical defect after LPAO was confirmed by our forced oscillatory data demonstrating marked elevations in Raw (Fig. 17). The lack of change in VDB following AE may be attributable to the relatively small amount of air reaching the pulmonary circulation (6%–8% of total intrapulmonary blood volume) that may have caused no major perfusion defects. Taken together with the findings from the computational study, this revealed that the lack of changes in VDB for the whole lung after LPAO can be explained by the development of severe hypocapnia-induced bronchoconstriction in the affected (left) lung, leading to the redistribution of VT to the contralateral unaffected (right) lung. This process may be accompanied by hypoxic pulmonary vasoconstriction in the occluded left lung, which further contributes to the uneven distribution of VDB.

41

9.3. Study limitations

9.3.1. Limitations of the anesthesia study

As a first limitation, our study comprised only male Sprague-Dawley rats. While males and female mice have previously been reported to have similar baseline respiratory mechanics when adjusted for body size [110], metabolic differences may influence the effects of various anesthetics. Sex differences have been found in the metabolic rate of pentobarbital [111], propofol [112; 113], and ketamine [114], with faster metabolism and higher doses needed in male rats or humans. While sex differences in the rate of metabolism of ketamine were also demonstrated, the effect of the actual plasma levels of various sex hormones was negligible [114]. No sex differences were found when using sevoflurane anesthesia in humans [113]. It is to be noted, though, that some studies have also described a faster metabolism in female humans when using propofol [115; 116]. Also, sex differences were found in mice in terms of airway responsiveness, with males showing significantly greater airway responses to MCh provocation [110].

Regarding different rat strains, differences can be expected in respiratory parameters (absolute values and in responsiveness of the animals) [117; 118; 119] and in metabolic and functional aspects of anesthesia [120; 121]. However, the baseline respiratory mechanical data presented in this study are in good agreement with those of previous studies using Wistar rats of the same size [36; 122].

All animals used in this study were considered to be young adults (body mass ranging between 280 g and 540 g, approximately 8–14 weeks of age). While most experiments include animals of a similar age and weight, the use of animals of differing ages may give different results due to age-related differences in anesthesia. This can manifest as dose differences and potentially differences in respiratory function. However, the observed differences in respiratory function between the different anesthetic regimes in this study are likely to be genuine as age-related differences in respiratory function are predominantly related to differences in body size.

This study comprised normal healthy rats without pathologies related to the respiratory or other organ systems. The presence of pathologic changes may alter the effects of anesthetic agents observed in this study, particularly when using rats as a model for respiratory diseases such as asthma, COPD or lung cancer.

The duration of the study protocol was limited. While the length of the experiments (approximately 2–2.5 hours) was similar to the most frequently used experimental protocols,

the examined outcomes may have differed with the use of a more prolonged experimental protocol, partly due to hemodynamical changes and heart-lung interactions.

Regarding the choice of anesthetics, the agents and their respective doses evaluated in this study were selected based on an extensive literature search and overview of the most commonly applied regimes. Accordingly, some anesthetic agents were used alone (urethane, pentobarbital and sevoflurane) as they have previously been shown to have appropriate analgesic effects in rodents [84; 123; 124]. Other agents were used in combinations. Propofol alone has an insufficient analgesic effect [125] and the combination of propofol with the opioid analgesic fentanyl is routinely used in human anesthesia. Ketamine is commonly used with xylazine in animal anesthesia due to their synergistic analgesic and anesthetic effects [126]. Since the effects of general anesthesia are dose-dependent [4], usage of different doses of the investigated agents can be a confounding variable and may be a subject of forthcoming investigations.

The current study aimed at characterizing the respiratory changes of animals undergoing general anesthesia with ventilatory support. While it is known that general anesthesia causes respiratory depression in a mostly dose-dependent manner [4], changes the breathing patterns [6; 7], and may result in lung volume loss via airway closure and atelectasis formation, the exact characterization of these phenomena in spontaneously breathing animals with the individual anesthesia regimes is beyond the scope of this study.

9.3.2. *Limitations of the embolism study*

A methodological consideration of the protocol for the embolism study is related to the protocol design, which focused on the acute consequences of PE. This approach allowed the comparison of two pulmonary circulatory insults in an animal model, thereby strengthening the statistical power and reducing the need for an excessive number of animals in accordance with the 3R principle. Indeed, complete recovery of monitored gas exchange ($ETCO_2$) and systemic circulatory parameters (MAP, HR) was observed between the interventions, which suggests the lack of a carryover effect between the protocol stages. However, the generalization of our findings to prolonged pulmonary perfusion defects should be considered. An additional limitation of this study is that volumetric capnography provides an overall picture about the ventilation-perfusion matching for the entire lungs. Expanded use of imaging techniques, such as SPECT [127], K-edge subtraction [128], electric impedance tomography [129], or quantitative ventilation-perfusion analysis by inert gas elimination [130] has the potential in forthcoming studies to further investigate the mechanisms by allowing regional assessments.

43

9. Summary and conclusions

This thesis presents a systematic comparison of the effects of commonly used anesthetic agents on the respiratory system at different PEEP levels and the lung's responsiveness to an exogenous constrictor stimulus.

Summarizing the effects of different anesthetic regimes on respiratory mechanics in rats, our findings led to the following conclusions:

I.   No differences were observed in baseline respiratory mechanics and function between the anesthesia regimes at any PEEP levels.

II.   Although baseline mechanical parameters were consistent, bronchial hyperreactivity developed under ketamine-xylazine anesthesia.

III.   The baseline respiratory mechanics of ventilated rats are not influenced by the commonly used anesthesia regimes at generally administered doses, allowing for a fair comparison among experimental animals undergoing different anesthesia protocols. Furthermore, ketamine-xylazine anesthesia may not be suitable for studies where bronchial reactivity is a critical component (e.g., sensitization studies).

The outcomes of the second study provide unique data on the differences between diffuse lung injury induced by intravenous injection of air bubbles, modeling gas embolism, and focal thromboembolism caused by clamping the left pulmonary artery. Regarding the effects of pulmonary air and thromboembolism on respiratory mechanics and ventilation-perfusion matching in rats, our findings led to these conclusions:

IV.   Deteriorations in lung mechanics, reflecting the development of heterogeneous bronchoconstriction, were observed after a focal ischemic insult to pulmonary perfusion. The severity of hypocapnia did not reach the threshold level to alter bronchial tone in any lung regions following a diffuse pulmonary perfusion defect subsequent to pulmonary air embolism.

V.   Contrasting with the mechanical changes, arterial blood gas parameters deteriorated following a diffuse pulmonary perfusion defect due to pulmonary air embolism, while focal perfusion defects due to pulmonary vascular occlusion triggered a compensatory respiratory mechanical response. This response led to airflow redistribution to lung areas with maintained perfusion, thereby maintaining normal oxygenation and CO_2 elimination. The different impacts of air and thromboembolism on lung mechanics and gas exchange may have implications in tailoring respiratory support for patients.

44

10. Acknowledgements

11. References

[1] Z. Csorba, F. Petak, K. Nevery, J. Tolnai, A.L. Balogh, F. Rarosi, G.H. Fodor, and B. Babik, Capnographic Parameters in Ventilated Patients: Correspondence with Airway and Lung Tissue Mechanics. Anesth Analg 122 (2016) 1412-20.

[2] C. Rhoades, and F. Thomas, Capnography: beyond the numbers. Air Med J 21 (2002) 43-8.

[3] J.H.T. Bates, CORP: Measurement of lung function in small animals. J Appl Physiol (1985) 123 (2017) 1039-1046.

[4] M.J. Fagerlund, Respiratory Depression. in: J.F.A. Hendrickx, and P.L. Gambús, (Eds.), Personalized Anaesthesia: Targeting Physiological Systems for Optimal Effect, Cambridge University Press, Cambridge, 2020, pp. 146-156.

[5] G.A. Hans, T.M. Sottiaux, M.L. Lamy, and J.L. Joris, Ventilatory management during routine general anaesthesia. Eur J Anaesthesiol 26 (2009) 1-8.

[6] G. Hedenstierna, and L. Edmark, The effects of anesthesia and muscle paralysis on the respiratory system. Intensive Care Med 31 (2005) 1327-35.

[7] B. Brismar, G. Hedenstierna, H. Lundquist, A. Strandberg, L. Svensson, and L. Tokics, Pulmonary densities during anesthesia with muscular relaxation--a proposal of atelectasis. Anesthesiology 62 (1985) 422-8.

[8] L. Tokics, G. Hedenstierna, A. Strandberg, B. Brismar, and H. Lundquist, Lung collapse and gas exchange during general anesthesia: effects of spontaneous breathing, muscle paralysis, and positive end-expiratory pressure. Anesthesiology 66 (1987) 157-67.

[9] W. Habre, F. Petak, P.D. Sly, Z. Hantos, and D.R. Morel, Protective effects of volatile agents against methacholine-induced bronchoconstriction in rats. Anesthesiology 94 (2001) 348-53.

[10] A.L. Balogh, F. Petak, G.H. Fodor, R. Sudy, and B. Babik, Sevoflurane Relieves Lung Function Deterioration After Cardiopulmonary Bypass. J Cardiothorac Vasc Anesth 31 (2017) 2017-2026.

[11] W. Habre, J.H. Wildhaber, and P.D. Sly, Prevention of methacholine-induced changes in respiratory mechanics in piglets: a comparison of sevoflurane and halothane. Anesthesiology 87 (1997) 585-90.

[12] H. Mitsuhata, J. Saitoh, R. Shimizu, H. Takeuchi, N. Hasome, and Y. Horiguchi, Sevoflurane and isoflurane protect against bronchospasm in dogs. Anesthesiology 81 (1994) 1230-4.

[13] M. Adam, J. Linden, M. Raekallio, A. Meller, B. Mannerstrom, A. Abu-Shahba, R. Seppanen-Kaijansinkko, and K. Salla, Effects of vatinoxan on xylazine-induced pulmonary alterations in sheep. J Vet Pharmacol Ther 45 (2022) 117-125.

[14] H.R. Amouzadeh, S. Sangiah, C.W. Qualls, Jr., R.L. Cowell, and A. Mauromoustakos, Xylazine-induced pulmonary edema in rats. Toxicol Appl Pharmacol 108 (1991) 417-27.

[15] Standards for Basic Anesthetic Monitoring, Retrieved on 10 February 2024 from, https://www.asahq.org/standards-and-practice-parameters/standards-for-basic-anesthetic-monitoring.

[16] B.C. Babik, Zs.; Balogh, Á.; Szenti, K.; Tolnai, J.; Petak, F., Kapnografia lélegeztetett betegekben. Mindig nézzük, mindent látunk? , Medicina Thoracalis, 2014, pp. 78-96.

[17] D.M. Garey, R. Ward, W. Rich, G. Heldt, T. Leone, and N.N. Finer, Tidal volume threshold for colorimetric carbon dioxide detectors available for use in neonates. Pediatrics 121 (2008) e1524-7.

[18] F.E. Block, Jr., and J.S. McDonald, Sidestream versus mainstream carbon dioxide analyzers. J Clin Monit 8 (1992) 139-41.

[19] R.C. Pascucci, J.A. Schena, and J.E. Thompson, Comparison of a sidestream and mainstream capnometer in infants. Crit Care Med 17 (1989) 560-2.

[20] N.L. Szaflarski, and N.H. Cohen, Use of capnography in critically ill adults. Heart Lung 20 (1991) 363-72.

[21] R. Fletcher, and B. Jonson, Deadspace and the single breath test for carbon dioxide during anaesthesia and artificial ventilation. Effects of tidal volume and frequency of respiration. Br J Anaesth 56 (1984) 109-19.

[22] G. Tusman, M. Areta, C. Climente, R. Plit, F. Suarez-Sipmann, M.J. Rodriguez-Nieto, G. Peces-Barba, E. Turchetto, and S.H. Bohm, Effect of pulmonary perfusion on the slopes of single-breath test of CO_2. J Appl Physiol (1985) 99 (2005) 650-5.

[23] E.O. Essien, P. Rali, and S.C. Mathai, Pulmonary Embolism. Med Clin North Am 103 (2019) 549-564.

[24] S. Doherty, Pulmonary embolism An update. Aust Fam Physician 46 (2017) 816-820.

[25] D. Bonderman, and I.M. Lang, End-tidal CO_2 for exclusion of suspected pulmonary embolism: a new partner for Wells? Eur Respir J 35 (2010) 723-4.

[26] J.E. Souders, J.B. Doshier, N.L. Polissar, and M.P. Hlastala, Spatial distribution of venous gas emboli in the lungs. J Appl Physiol (1985) 87 (1999) 1937-47.

[27] A.J. Calderon, J.B. Fowlkes, and J.L. Bull, Bubble splitting in bifurcating tubes: a model study of cardiovascular gas emboli transport. J Appl Physiol (1985) 99 (2005) 479-87.

[28] H.K. Chang, L. Delaunois, R. Boileau, and R.R. Martin, Redistribution of pulmonary blood flow during experimental air embolism. J Appl Physiol Respir Environ Exerc Physiol 51 (1981) 211-7.

[29] M.K. Atalay, N.L. Walle, D.J. Grand, W.W. Mayo-Smith, J.J. Cronan, and T.K. Egglin, Scan length optimization for pulmonary embolism at CT angiography: analysis based on the three-dimensional spatial distribution of 370 emboli in 100 patients. Clin Radiol 66 (2011) 405-11.

[30] J.Y. Tsang, W.J. Lamm, I.R. Starr, and M.P. Hlastala, Spatial pattern of ventilation-perfusion mismatch following acute pulmonary thromboembolism in pigs. J Appl Physiol (1985) 98 (2005) 1862-8.

[31] J. Zhang, Y. Chen, Z. Wang, X. Chen, Y. Liu, and M. Liu, Anatomic distribution of lower extremity deep venous thrombosis is associated with an increased risk of pulmonary embolism: A 10-year retrospective analysis. Front Cardiovasc Med 10 (2023) 1154875.

[32] Z. Hantos, B. Daroczy, B. Suki, S. Nagy, and J.J. Fredberg, Input impedance and peripheral inhomogeneity of dog lungs. J Appl Physiol (1985) 72 (1992) 168-78.

[33] N. Percie du Sert, V. Hurst, A. Ahluwalia, S. Alam, M.T. Avey, M. Baker, W.J. Browne, A. Clark, I.C. Cuthill, U. Dirnagl, M. Emerson, P. Garner, S.T. Holgate, D.W. Howells, N.A. Karp, S.E. Lazic, K. Lidster, C.J. MacCallum, M. Macleod, E.J. Pearl, O.H. Petersen, F. Rawle, P. Reynolds, K. Rooney, E.S. Sena, S.D. Silberberg, T. Steckler, and H. Wurbel, The ARRIVE guidelines 2.0: Updated guidelines for reporting animal research. PLoS Biol 18 (2020) e3000410.

[34] T.Z. Janosi, A. Adamicza, G.R. Zosky, T. Asztalos, P.D. Sly, and Z. Hantos, Plethysmographic estimation of thoracic gas volume in apneic mice. J Appl Physiol (1985) 101 (2006) 454-9.

[35] F. Petak, Z. Hantos, A. Adamicza, T. Asztalos, and P.D. Sly, Methacholine-induced bronchoconstriction in rats: effects of intravenous vs. aerosol delivery. J Appl Physiol (1985) 82 (1997) 1479-87.

[36] A. Schranc, G.H. Fodor, R. Sudy, B. Ballok, R. Kulcsar, J. Tolnai, B. Babik, and F. Petak, Lung and chest wall mechanical properties in metformin-treated and untreated models of type 2 diabetes. J Appl Physiol (1985) 132 (2022) 1115-1124.

47

[37] G.H. Fodor, W. Habre, A.L. Balogh, R. Sudy, B. Babik, and F. Petak, Optimal crystalloid volume ratio for blood replacement for maintaining hemodynamic stability and lung function: an experimental randomized controlled study. BMC Anesthesiol 19 (2019) 21.

[38] H. Franken, J. Clement, M. Cauberghs, and K.P. Van de Woestijne, Oscillating flow of a viscous compressible fluid through a rigid tube: a theoretical model. IEEE Trans Biomed Eng 28 (1981) 416-20.

[39] F. Petak, G.L. Hall, and P.D. Sly, Repeated measurements of airway and parenchymal mechanics in rats by using low-frequency oscillations. J Appl Physiol 84 (1998) 1680-6.

[40] J. Tolnai, G.H. Fodor, B. Babik, A. Dos Santos Rocha, S. Bayat, F. Petak, and W. Habre, Volumetric but Not Time Capnography Detects Ventilation/Perfusion Mismatch in Injured Rabbit Lung. Front Physiol 9 (2018) 1805.

[41] G. Tusman, A. Scandurra, S.H. Bohm, F. Suarez-Sipmann, and F. Clara, Model fitting of volumetric capnograms improves calculations of airway dead space and slope of phase III. J Clin Monit Comput 23 (2009) 197-206.

[42] R.S. Ream, M.S. Schreiner, J.D. Neff, K.M. McRae, A.F. Jawad, P.W. Scherer, and G.R. Neufeld, Volumetric capnography in children. Influence of growth on the alveolar plateau slope. Anesthesiology 82 (1995) 64-73.

[43] N.M. Tsoukias, Z. Tannous, A.F. Wilson, and S.C. George, Single-exhalation profiles of NO and CO2 in humans: effect of dynamically changing flow rate. J Appl Physiol (1985) 85 (1998) 642-52.

[44] W.S. Fowler, Lung function studies; the respiratory dead space. Am J Physiol 154 (1948) 405-16.

[45] C. Bohr, Über die Lungenatmung. Skan Arch Physiol (1891) 236-238.

[46] E. H, Volumen inefficax. Uppsala Laekareforen Forh (1938) 191-218.

[47] F. Suarez-Sipmann, S.H. Bohm, and G. Tusman, Volumetric capnography: the time has come. Curr Opin Crit Care 20 (2014) 333-9.

[48] M.A. Rodger, C.N. Bredeson, G. Jones, P. Rasuli, F. Raymond, A.M. Clement, A. Karovitch, H. Brunette, D. Makropoulos, M. Reardon, I. Stiell, R. Nair, and P.S. Wells, The bedside investigation of pulmonary embolism diagnosis study: a double-blind randomized controlled trial comparing combinations of 3 bedside tests vs ventilation-perfusion scan for the initial investigation of suspected pulmonary embolism. Arch Intern Med 166 (2006) 181-7.

[49] S.K. Wixson, and K.L. Smiler, Chapter 9: Anesthesia and Analgesia in Rodents. in: D.F. Kohn, S.K. Wixson, W.J. White, and G.J. Benson, (Eds.), Anesthesia and Analgesia in Laboratory Animals, Elsevier Ltd., 1997, pp. 193-195.

[50] D. Obal, B. Preckel, H. Scharbatke, J. Mullenheim, F. Hoterkes, V. Thamer, and W. Schlack, One MAC of sevoflurane provides protection against reperfusion injury in the rat heart in vivo. Br J Anaesth 87 (2001) 905-11.

[51] Y.G. Lee, J.L. Kim, A.F. Palmer, B.F. Reader, J. Ma, S.M. Black, and B.A. Whitson, A Rat Lung Transplantation Model of Warm Ischemia/Reperfusion Injury: Optimizations to Improve Outcomes. J Vis Exp (2021).

[52] R. Sudy, G.H. Fodor, A. Dos Santos Rocha, A. Schranc, J. Tolnai, W. Habre, and F. Petak, Different contributions from lungs and chest wall to respiratory mechanics in mice, rats, and rabbits. J Appl Physiol (1985) 127 (2019) 198-204.

[53] R. Bausell, and Y. Li, Power Analysis for Experimental Research: A Practical Guide for the Biological, Medical and Social Sciences. Cambridge: Cambridge University Press (2002).

[54] E.E. Lele, Z. Hantos, M. Bitay, B. Szivos, G. Bogats, F. Petak, and B. Babik, Bronchoconstriction during alveolar hypocapnia and systemic hypercapnia in dogs with a cardiopulmonary bypass. Respir Physiol Neurobiol 175 (2011) 140-5.

[55] G.H. Fodor, B. Babik, D. Czovek, C. Doras, A.L. Balogh, S. Bayat, W. Habre, and F. Petak, Fluid replacement and respiratory function: comparison of whole blood with colloid and crystalloid: A randomised animal study. Eur J Anaesthesiol 33 (2016) 34-41.

[56] C.R. Brown, W.H. Forrest, Jr., and J. Hayden, The respiratory effects of pentobarbital and secobarbital in clinical doses. J Clin Pharmacol New Drugs 13 (1973) 28-35.

[57] J.C. Gasser, R.D. Kaufman, and J.W. Bellville, Respiratory effects of lorazepam, pentobarbital, and pentazocine. Clin Pharmacol Ther 18 (1975) 170-4.

[58] J. Jiang, Y. Jiao, P. Gao, W. Yin, W. Zhou, Y. Zhang, Y. Liu, D. Wen, Y. Wang, L. Zhou, T. Yu, and W. Yu, Propofol differentially induces unconsciousness and respiratory depression through distinct interactions between GABAA receptor and GABAergic neuron in corresponding nuclei. Acta Biochim Biophys Sin (Shanghai) 53 (2021) 1076-1087.

[59] A. Peratoner, C.S. Nascimento, M.C. Santana, R.A. Cadete, E.M. Negri, A. Gullo, P.R. Rocco, and W.A. Zin, Effects of propofol on respiratory mechanic and lung histology in normal rats. Br J Anaesth 92 (2004) 737-40.

[60] B.S. von Ungern-Sternberg, S. Saudan, F. Petak, Z. Hantos, and W. Habre, Desflurane but not sevoflurane impairs airway and respiratory tissue mechanics in children with susceptible airways. Anesthesiology 108 (2008) 216-24.

[61] C.A. Volta, V. Alvisi, S. Petrini, S. Zardi, E. Marangoni, R. Ragazzi, M. Capuzzo, and R. Alvisi, The effect of volatile anesthetics on respiratory system resistance in patients with chronic obstructive pulmonary disease. Anesth Analg 100 (2005) 348-353.

[62] F.C. Correa, P.B. Ciminelli, H. Falcao, B.J. Alcantara, R.S. Contador, A.S. Medeiros, W.A. Zin, and P.R. Rocco, Respiratory mechanics and lung histology in normal rats anesthetized with sevoflurane. J Appl Physiol (1985) 91 (2001) 803-10.

[63] R.H. Brown, and E.M. Wagner, Mechanisms of bronchoprotection by anesthetic induction agents: propofol versus ketamine. Anesthesiology 90 (1999) 822-8.

[64] E. Lele, F. Petak, S. Carnesecchi, K. Virag, C.B. Argiroffo, and W. Habre, The protective effects of volatile anesthestics against the bronchoconstriction induced by an allergic reaction in sensitized rabbit pups. Anesth Analg 116 (2013) 1257-64.

[65] N.L. Biddle, A.W. Gelb, and J.T. Hamilton, Propofol differentially attenuates the responses to exogenous and endogenous norepinephrine in the isolated rat femoral artery in vitro. Anesth Analg 80 (1995) 793-9.

[66] O. Gateau, J.L. Bourgain, J.H. Gaudy, and J. Benveniste, Effects of ketamine on isolated human bronchial preparations. Br J Anaesth 63 (1989) 692-5.

[67] P.H. Leblanc, C.K. Buckner, D.B. Brunson, R.B. Laravuso, and J.A. Will, Differential effect of ketamine on cholinergic- and noncholinergic-induced contractions of isolated guinea-pig bronchi. Arch Int Pharmacodyn Ther 287 (1987) 120-32.

[68] M.J. Rock, S. Reyes de la Rocha, M. Lerner, D. Brackett, and M.F. Wilson, Effect on airway resistance of ketamine by aerosol in guinea pigs. Anesth Analg 68 (1989) 506-10.

[69] M.M. Zhu, Q.H. Zhou, M.H. Zhu, H.B. Rong, Y.M. Xu, Y.N. Qian, and C.Z. Fu, Effects of nebulized ketamine on allergen-induced airway hyperresponsiveness and inflammation in actively sensitized Brown-Norway rats. J Inflamm (Lond) 4 (2007) 10.

[70] G.C. Watney, L.W. Hall, C. Jordan, and A.M. Nolan, Effects of xylazine and acepromazine on bronchomotor tone of anaesthetised ponies. Equine Vet J 20 (1988) 185-8.

[71] K.R. Lutchen, Z. Hantos, F. Petak, A. Adamicza, and B. Suki, Airway inhomogeneities contribute to apparent lung tissue mechanics during constriction. J Appl Physiol (1985) 80 (1996) 1841-9.

[72] O. Alves-Neto, P. Tavares, P.R. Rocco, and W.A. Zin, Respiratory mechanics and morphometric changes during anesthesia with ketamine in normal rats. Braz J Med Biol Res 34 (2001) 1217-23.

[73] N. Schutz, F. Petak, C. Barazzone-Argiroffo, F. Fontao, and W. Habre, Effects of volatile anaesthetic agents on enhanced airway tone in sensitized guinea pigs. Br J Anaesth 92 (2004) 254-60.

[74] A. Sanchez-Pozo, J.C. Alados, and F. Sanchez-Medina, Metabolic changes induced by urethane-anesthesia in rats. Gen Pharmacol 19 (1988) 281-4.

[75] K. Takeuchi, H. Niida, T. Ohuchi, and S. Okabe, Influences of urethane anesthesia on indomethacin-induced gastric mucosal lesions in rats. Relation to blood glucose levels. Dig Dis Sci 39 (1994) 2536-42.

[76] K. Aisaka, T. Kihara, M. Koike, M. Kuroki, and T. Ishihara, Effect of yohimbine on urethane-induced hyperglycemia in rats. Jpn J Pharmacol 49 (1989) 523-7.

[77] C.F. Reyes Toso, L.M. Linares, and R.R. Rodriguez, Blood sugar concentrations during ketamine or pentobarbitone anesthesia in rats with or without alpha and beta adrenergic blockade. Medicina (B Aires) 55 (1995) 311-6.

[78] C.J. Zuurbier, A. Koeman, S.M. Houten, M.W. Hollmann, and W.J. Florijn, Optimizing anesthetic regimen for surgery in mice through minimization of hemodynamic, metabolic, and inflammatory perturbations. Exp Biol Med (Maywood) 239 (2014) 737-46.

[79] E.P. Steffey, P.J. Pascoe, M.J. Woliner, and E.R. Berryman, Effects of xylazine hydrochloride during isoflurane-induced anesthesia in horses. Am J Vet Res 61 (2000) 1225-31.

[80] F. Safaei, E. Tamaddonfard, S. Nafisi, and M. Imani, Effects of intraperitoneal and intracerebroventricular injection of cinnamaldehyde and yohimbine on blood glucose and serum insulin concentrations in ketamine-xylazine induced acute hyperglycemia. Vet Res Forum 12 (2021) 149-156.

[81] C.J. Zuurbier, Ketamine-(Dex)Medetomidine, Hyperglycemia, Glycocalyx, and Vascular Permeability. Anesth Analg 129 (2019) e102.

[82] A. Brammer, C.D. West, and S.L. Allen, A comparison of propofol with other injectable anaesthetics in a rat model for measuring cardiovascular parameters. Lab Anim 27 (1993) 250-7.

[83] P.F. Conzen, B. Vollmar, H. Habazettl, E.J. Frink, K. Peter, and K. Messmer, Systemic and regional hemodynamics of isoflurane and sevoflurane in rats. Anesth Analg 74 (1992) 79-88.

[84] D.J. De Wildt, F.C. Hillen, A.G. Rauws, and B. Sangster, Etomidate-anaesthesia, with and without fentanyl, compared with urethane-anaesthesia in the rat. Br J Pharmacol 79 (1983) 461-9.

[85] N. Himori, and T. Ishimori, Different responses to beta-adrenoceptor blocking drugs of the blood pressure and heart rate in the urethane-anesthetized dog and rat. Jpn J Pharmacol 47 (1988) 71-80.

[86] J.I. Fortea, M. Puerto, C. Fernandez-Mena, I. Asensio, M. Arriba, J. Almagro, J. Banares, C. Ripoll, R. Banares, and J. Vaquero, Sevoflurane versus ketamine+diazepam anesthesia for assessing systemic and hepatic hemodynamics in rats with non-cirrhotic portal hypertension. PLoS One 15 (2020) e0233778.

[87] M. Albrecht, J. Henke, S. Tacke, M. Markert, and B. Guth, Influence of repeated anaesthesia on physiological parameters in male Wistar rats: a telemetric study about

isoflurane, ketamine-xylazine and a combination of medetomidine, midazolam and fentanyl. BMC Vet Res 10 (2014) 310.

[88] C. Wang, J. Jin Lee, H.H. Jung, and Z. Zuo, Pretreatment with volatile anesthetics, but not with the nonimmobilizer 1,2-dichlorohexafluorocyclobutane, reduced cell injury in rat cerebellar slices after an in vitro simulated ischemia. Brain Res 1152 (2007) 201-8.

[89] D. Schifilliti, G. Grasso, A. Conti, and V. Fodale, Anaesthetic-related neuroprotection: intravenous or inhalational agents? CNS Drugs 24 (2010) 893-907.

[90] W.E. Hoffman, F.T. Charbel, G. Edelman, and J.I. Ausman, Thiopental and desflurane treatment for brain protection. Neurosurgery 43 (1998) 1050-3.

[91] M. Kobayashi, Y. Takeda, H. Taninishi, K. Takata, H. Aoe, and K. Morita, Quantitative evaluation of the neuroprotective effects of thiopental sodium, propofol, and halothane on brain ischemia in the gerbil: effects of the anesthetics on ischemic depolarization and extracellular glutamate concentration. J Neurosurg Anesthesiol 19 (2007) 171-8.

[92] T. Sakai, T. Ichiyama, C.W. Whitten, A.H. Giesecke, and J.M. Lipton, Ketamine suppresses endotoxin-induced NF-kappaB expression. Can J Anaesth 47 (2000) 1019-24.

[93] C.A. Maggi, and A. Meli, Suitability of urethane anesthesia for physiopharmacological investigations in various systems. Part 1: General considerations. Experientia 42 (1986) 109-14.

[94] S. Pagliardini, G.D. Funk, and C.T. Dickson, Breathing and brain state: urethane anesthesia as a model for natural sleep. Respir Physiol Neurobiol 188 (2013) 324-32.

[95] M. Arslan, Z. Ozkose, G. Akyol, and G. Barit, The age- and gender-dependent effects of desflurane and sevoflurane on rat liver. Exp Toxicol Pathol 62 (2010) 35-43.

[96] F. Huang, S. Li, X. Gan, R. Wang, and Z. Chen, Propofol inhibits gap junctions by attenuating sevoflurane-induced cytotoxicity against rat liver cells in vitro. Eur J Anaesthesiol 31 (2014) 219-24.

[97] B.M.N.I.o.D.a.D.a.K. Diseases, LiverTox: Clinical and Research Information on Drug-Induced Liver Injury [Internet], https://www.ncbi.nlm.nih.gov/books/NBK547852/, 2012-.

[98] F. Sozio, T. Schioppa, S. Sozzani, and A. Del Prete, Urethane-induced lung carcinogenesis. Methods Cell Biol 163 (2021) 45-57.

[99] G. Du, T. Sun, Y. Zhang, H. Lin, J. Li, W. Liu, Y. Wang, B. Zhao, H. Li, and Y. Liu, The mitochondrial dysfunction plays an important role in urethane-induced lung carcinogenesis. Eur J Pharmacol 715 (2013) 395-404.

[100] D.W. Kaczka, R.H. Brown, and W. Mitzner, Assessment of heterogeneous airway constriction in dogs: a structure-function analysis. J Appl Physiol (1985) 106 (2009) 520-30.

[101] D. Fors, K. Eiriksson, D. Arvidsson, and S. Rubertsson, Gas embolism during laparoscopic liver resection in a pig model: frequency and severity. Br J Anaesth 105 (2010) 282-8.

[102] M. Simon, B. Battistini, Y. Joo Kim, and J. Tsang, Plasma levels of endothelin-1, big endothelin-1 and thromboxane following acute pulmonary air embolism. Respir Physiol Neurobiol 138 (2003) 97-106.

[103] S. Deem, S. McKinney, N.L. Polissar, R.G. Hedges, and E.R. Swenson, Hemodilution during venous gas embolization improves gas exchange, without altering V(A)/Q or pulmonary blood flow distributions. Anesthesiology 91 (1999) 1861-72.

[104] G. Hedenstierna, and B. Sandhagen, Assessing dead space. A meaningful variable? Minerva Anestesiol 72 (2006) 521-8.

[105] C.G. Elliott, Pulmonary physiology during pulmonary embolism. Chest 101 (1992) 163S-171S.

[106] V.L. Hoellerich, and R.S. Wigton, Diagnosing pulmonary embolism using clinical findings. Arch Intern Med 146 (1986) 1699-704.

[107] J. Petersson, and R.W. Glenny, Gas exchange and ventilation-perfusion relationships in the lung. Eur Respir J 44 (2014) 1023-41.

[108] J.R. Mondonedo, J.S. McNeil, J. Herrmann, B.A. Simon, and D.W. Kaczka, Targeted Versus Continuous Delivery of Volatile Anesthetics During Cholinergic Bronchoconstriction. J Eng Sci Med Diagn Ther 1 (2018) 031003-1-031003-10.

[109] M.S. Siobal, H. Ong, J. Valdes, and J. Tang, Calculation of physiologic dead space: comparison of ventilator volumetric capnography to measurements by metabolic analyzer and volumetric CO2 monitor. Respir Care 58 (2013) 1143-51.

[110] J.W. Card, M.A. Carey, J.A. Bradbury, L.M. DeGraff, D.L. Morgan, M.P. Moorman, G.P. Flake, and D.C. Zeldin, Gender differences in murine airway responsiveness and lipopolysaccharide-induced inflammation. J Immunol 177 (2006) 621-30.

[111] E.A. Zambricki, and L.G. Dalecy, Rat sex differences in anesthesia. Comp Med 54 (2004) 49-53.

[112] M. Mukai, T. Isobe, K. Okada, M. Murata, M. Shigeyama, and N. Hanioka, Species and sex differences in propofol glucuronidation in liver microsomes of humans, monkeys, rats and mice. Pharmazie 70 (2015) 466-70.

[113] M. Kodaka, J.W. Johansen, and P.S. Sebel, The influence of gender on loss of consciousness with sevoflurane or propofol. Anesth Analg 101 (2005) 377-381.

[114] S.K. Saland, and M. Kabbaj, Sex Differences in the Pharmacokinetics of Low-dose Ketamine in Plasma and Brain of Male and Female Rats. J Pharmacol Exp Ther 367 (2018) 393-404.

[115] S. Maeda, Y. Tomoyasu, H. Higuchi, Y. Honda, M. Ishii-Maruhama, and T. Miyawaki, Female Patients Require a Higher Propofol Infusion Rate for Sedation. Anesth Prog 63 (2016) 67-70.

[116] H. Pleym, O. Spigset, E.D. Kharasch, and O. Dale, Gender differences in drug effects: implications for anesthesiologists. Acta Anaesthesiol Scand 47 (2003) 241-59.

[117] Y. Nakano, M. Yokohira, N. Hashimoto, K. Yamakawa, S. Kishi, F. Ninomiya, S. Kanie, K. Saoo, and K. Imaida, Rat strain differences in levels and effects of chronic inflammation due to intratracheal instillation of quartz on lung tumorigenesis induced by DHPN. Exp Toxicol Pathol 66 (2014) 391-401.

[118] R.L. Boyd, L.W. Halderman, J.O. Harris, and J.A. Mangos, Strain differences in pulmonary function of laboratory rats. Lab Anim Sci 32 (1982) 42-3.

[119] P. Baumann, S. Wiegert, F. Greco, J. Ersch, and V. Cannizzaro, Strain-specific differences in lung tissue viscoelasticity of mechanically ventilated infant Sprague-Dawley and Wistar rats. Am J Physiol Lung Cell Mol Physiol 320 (2021) L220-L231.

[120] H. Avsaroglu, A.S. van der Sar, H.A. van Lith, L.F. van Zutphen, and L.J. Hellebrekers, Differences in response to anaesthetics and analgesics between inbred rat strains. Lab Anim 41 (2007) 337-44.

[121] D. Gong, Z. Fang, P. Ionescu, M.J. Laster, R.C. Terrell, and E.I. Eger, 2nd, Rat strain minimally influences anesthetic and convulsant requirements of inhaled compounds in rats. Anesth Analg 87 (1998) 963-6.

[122] R. Sudy, A. Schranc, G.H. Fodor, J. Tolnai, B. Babik, and F. Petak, Lung volume dependence of respiratory function in rodent models of diabetes mellitus. Respir Res 21 (2020) 82.

[123] J.N. Reimer, C.J. Schuster, C.G. Knight, D.S.J. Pang, and V.S.Y. Leung, Intraperitoneal injection of sodium pentobarbital has the potential to elicit pain in adult rats (Rattus norvegicus). PLoS One 15 (2020) e0238123.

[124] Y. Inada, Y. Funai, H. Yamasaki, T. Mori, and K. Nishikawa, Effects of sevoflurane and desflurane on the nociceptive responses of substantia gelatinosa neurons in the rat spinal cord dorsal horn: An in vivo patch-clamp analysis. Mol Pain 16 (2020) 1744806920903149.

[125] T. Goto, J.J. Marota, and G. Crosby, Pentobarbitone, but not propofol, produces pre-emptive analgesia in the rat formalin model. Br J Anaesth 72 (1994) 662-7.

[126] C.A. Richardson, and P.A. Flecknell, Anaesthesia and post-operative analgesia following experimental surgery in laboratory rodents: are we making progress? Altern Lab Anim 33 (2005) 119-27.

[127] A. Dos Santos Rocha, G.H. Fodor, M. Kassai, L. Degrugilliers, S. Bayat, F. Petak, and W. Habre, Physiologically variable ventilation reduces regional lung inflammation in a pediatric model of acute respiratory distress syndrome. Respir Res 21 (2020) 288.

[128] L. Porra, L. Degrugilliers, L. Broche, G. Albu, S. Strengell, H. Suhonen, G.H. Fodor, F. Petak, P. Suortti, W. Habre, A.R.A. Sovijarvi, and S. Bayat, Quantitative Imaging of Regional Aerosol Deposition, Lung Ventilation and Morphology by Synchrotron Radiation CT. Sci Rep 8 (2018) 3519.

[129] M. Xu, H. He, and Y. Long, Lung Perfusion Assessment by Bedside Electrical Impedance Tomography in Critically Ill Patients. Front Physiol 12 (2021) 748724.

[130] M. Edlinger-Stanger, M.H. Bernardi, K. Kovacs, M. Mascha, T. Neugebauer, S. Bohme, N. Ayoubi, N. Christofi, J. Garry, N. Fleming, and M. Hiesmayr, The effect of acute ventilation-perfusion mismatch on respiratory heat exchange in a porcine model. PLoS One 16 (2021) e0254399.